NOTE TO USERS

Effect of Local Material Properties on Tapping Mode Atomic Force Microscopy

Wensheng Xu

A Thesis

in

The Department

of

Mechanical and Industrial Engineering

Presented in Partial Fulfilment of the Requirements
for the Degree of Master of Applied Science (Mechanical Engineering) at
Concordia University
Montreal, Quebec, Canada

August 2005

Your file Votre référence
ISBN: 0-494-10276-4
Our file Notre référence
ISBN: 0-494-10276-4

ABSTRACT

Effect of Local Material Properties on Tapping Mode Atomic Force Microscopy

Wensheng Xu

The phase image produced by Atomic Force Microscopy (AFM) is very important in the study of surface topography and properties. The phase difference of different domains on a surface is due to the different tip-sample interaction forces which are a consequence of different local properties. By simulating the AFM imaging procedure and the tip-sample interactions with variable viscosity and modulus, the effect of local material properties on phase lag was studied. These simulations showed that both elastic and viscous properties have an influence on the phase lag. For hard, elastic materials the dominant interaction force is the elastic force, and for soft, viscoelastic materials the viscous force is dominant. The phase lag between the probe response and the activation force is higher for soft viscoelstic domains. With the mathematical model it was demonstrated that the phase contrast between viscoelastic materials and silicon can be used to predict the local viscosity and elastic modulus.

Experiments were done on a surface with a silicon domain which is hard and elastic and different viscoelastic domains. The experimental results of polybutadiene and polystyrene agree well with the simulation. The model was also applied to a block copolymer of butadiene and styrene and crystalline and amorphous polylactic acid. Finally, it is demonstrated that the AFM can detect materials properties beneath the surface.

ACKNOWLEDGEMENTS

I want to thank my supervisor Dr. Paula Wood-Adams for writing this thesis with me. I also acknowledge Dr. S. Rakheja, Dr. L. Cuccia, Dr.M. Medraj, and Dr. R. Sedaghati for acting on my examination committee, my colleagues W. Heng, F. Ark, H. Cheng, Y. Yury for giving me help during experiments, Dr. Robertson for providing the PB data, Dr. Luis Rodrigues for giving me advice on simulation. This thesis obtained founding from Taiho Kogyo Tribology Research Foundation.

Table of Contents

List of Figures

List of Tables

List of Nomenclature

A	set point amplitude
A_0	free vibration amplitude
a_0	interatomic distance
D	tip-sample distance
E	Young's modulus
E_t	Young's modulus of the tip
E_s	Young's modulus of the sample
E^*	Young's modulus of the tip-sample contact
E_{ext}	energy from the excitation force,
E_{med}	energy dissipated in the environment
E_{dis}	energy dissipated on the sample surface
c_0	damping coefficients of the oscillator in the air
c_{visc}	damping coefficient related to the viscous force
c_{NC}	damping coefficient related to van der Waals force
F_0	activation force amplitude
F_{ts}	tip-sample interaction force
F_{vis}	viscous force
G	elastic modulus
G_e	equilibrium modulus
G'	storage modulus
G''	loss modulus
H	Hamaker constant
h	thickness of the sample
k	spring constant
M_W	weight-average molar mass
M_N	number-average molar mass
p	the pressure
Q	quality factor
R	tip radius
R_e	Reynolds number
t	time
V_t	tip velocity
v_s	Poisson's coefficient of the sample
v_t	Poisson's coefficients of the tip
z	instantaneous tip position
z_c	probe-surface separation

η	viscosity
γ_{21}	shear strain
γ_0	shear strain amplitude
τ_{21}	shear stress
ω	angular frequency
η^*	complex viscosity
γ	surface energy
δ	indentation depth of tip into the surface
ρ	density
η_m	monomer viscosity
ϕ	phase of probe response
τ_{res}	time when the tip interacts with the sample

1. Introduction

The main objective of this work is to study the influence of material properties on atomic force microscopy (AFM) and develop a model to describe this influence. Therefore, the first issue is to understand how the AFM works.

1.1 Principle of operation in Atomic force microscopy (AFM)

AFM is a new microscopic technique based on a different operation principle from electron and optical microscopy. [1] Fig. 1-1 shows an example to explain how the AFM obtains the topography information from a sample surface. In this example a balloon flying over a mountain is considered. If people in the balloon use the height meter to check the distance between the balloon and the surface all the time and adjust the balloon up and down to maintain a constant distance between the balloon and the surface, the recorded flying trace will be the same as the topography of surface.

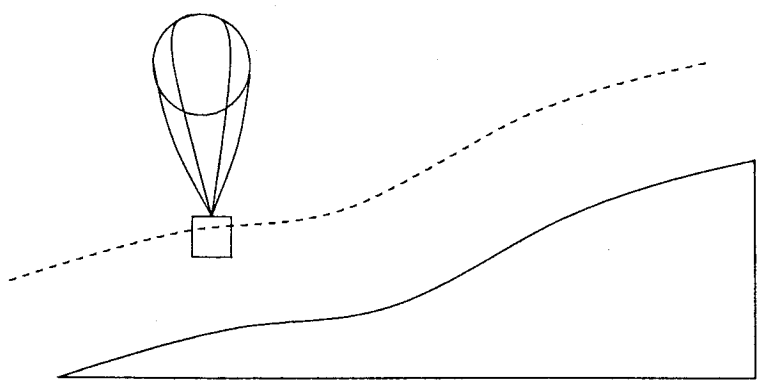

Figure 1-1 Balloon flying over mountain at a constant distance from the surface

For AFM, the relative movement of a probe and sample is like that of the balloon and the mountain. The adjustment of the distance between the probe and sample is done

by a feedback loop working like the person in the balloon. Instead of a height meter, the AFM uses the tip of the probe to touch the sample surface and sense the tip-sample interaction giving the distance between the tip and surface. As the tip-sample interaction changes with topography, the feedback loop of AFM adjusts the vertical position of the sample thus controlling the tip-sample interaction at its set point. The history of the vertical movement of the sample is like the trace of the flying balloon and is used to draw the topography image.

AFM has many advantages compared to electron and optical microscopy. It can produce a higher resolution image. It can provide a three dimensional topography map of the surface. The sample is easier to prepare. Finally, the experiments can be done when the sample is in different gaseous or liquid environments.[1,2] For these reasons, it is widely used in the study of materials.

When Scanning probe microscopy was first invented by Binnig in 1981, it used a probe near a surface to sense the tunnel current change between the tip and surface and was also called scanning tunnel microcopy (STM).[2] Because the tunnel current strongly depends on the tip-sample separation distance, STM is sensitive and can produce high resolution topography images. However, it can only be used on conductive materials. The appearance of contact mode AFM solved this problem. In this mode, the tip of the probe actually contacts the sample surface resulting in a mechanical tip-sample interaction force. A change in the tip-sample force leads to a deflection in the cantilever upon which the tip is mounted. By using the cantilever deflection as a feedback loop signal, the topography is obtained. Contact mode AFM is widely used in the surface study of polymers which are not conductive. Moreover, contact mode AFM can also provide some information

about material properties like friction because of different forces occurring between the tip and different materials. [1-3]

Tapping mode AFM is a new development of AFM. [1, 2] Unlike the static probe of the contact mode, it uses a probe that vibrates at a constant frequency to scan over the material surface. The vibration amplitude changes as the probe-sample interaction forces change. Using the amplitude as a feedback loop signal, the tip-sample separation distance remains fixed and the topography image is drawn. Compared to contact mode, tapping mode does not damage as much the surface of soft materials because the tip intermittently contacts the surface without scratching it. Tapping mode AFM provides more information about material properties because the tip-sample interaction forces influence not only the amplitude; they also influence the phase of the probe response with respect to the activation force, which is explained in the following. Hence, the phase of the probe response contains the information of the material properties. [1-7]

1.2 Principle of topography and phase imaging in tapping mode AFM

The tapping mode AFM system is composed of a silicon probe, a laser generator, a photodetector, a controller, a scanner and a probe holder with piezoelectric drivers, shown in Fig. 1-2. At first, the controller gives an oscillation signal to the piezoelectric material under the probe to make the probe vibrate near its resonance frequency. The laser focused on the back of the probe is reflected to the photodetector. Movements of the laser beam are detected by the photodetector and a signal is sent to the controller. The value of this signal represents the amplitude of the probe vibration. When the tip scans

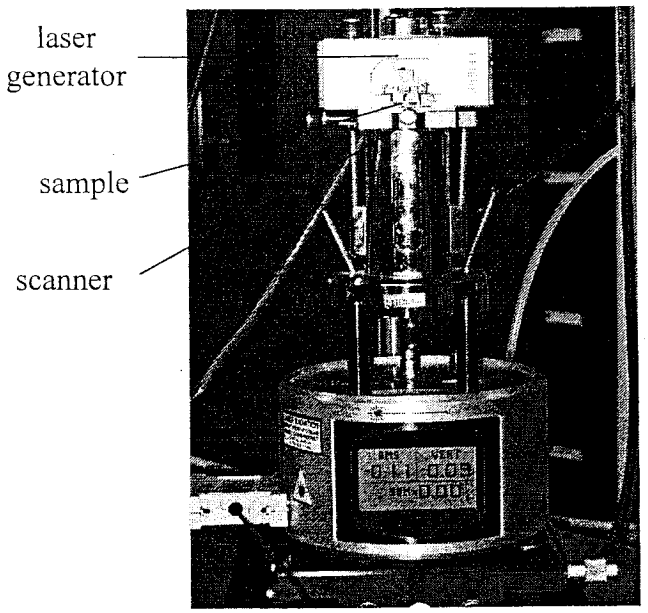

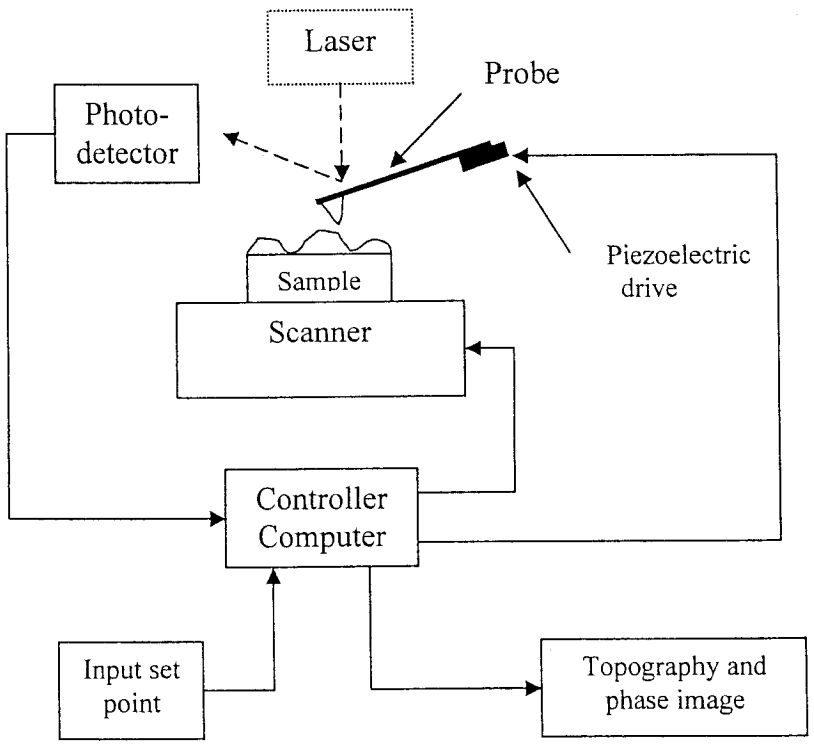

Figure 1-2 The AFM system

the sample surface, the vibration amplitude will be affected by the topography. Any change is detected by a photodetector and a signal is sent to the controller. The controller compares the detected signal to the set point value and generates an error signal. This error signal is processed and changed into a voltage signal by the controller and then sent to the scanner resulting in an adjustment of the tip-sample separation distance which returns the probe vibration amplitude to the set point value. This adjustment of the scanner is recorded and used to produce the topography image. At the same time, the phase of the probe response with respect to the activation force is recorded and used to produce the phase image. Because the probe response is always lagging the activation signal, we use the activation force as the reference to calculate the phase lag of the probe response. The phase lag of the probe response with respect to the exciting force is called the "phase of the probe response" (shown in Fig.1-3) in this thesis for convenience (the meaning of phase here is different from that in material science). The phase image is a 2-dimensional map of the phase of the probe response. Fig.1-4 shows a phase image for polybutadiene (PB) and silicon surface.

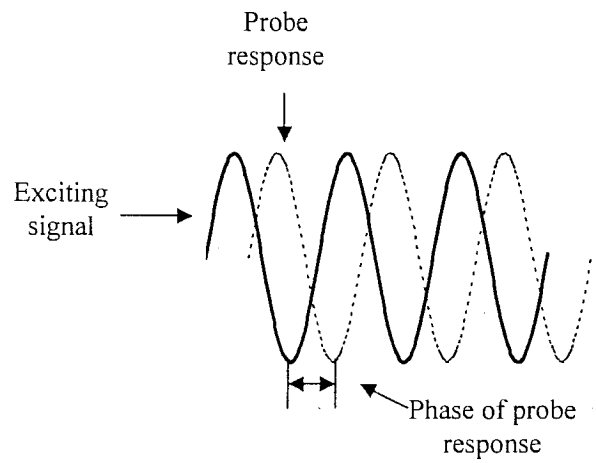

Figure 1-3 Phase shift of probe response

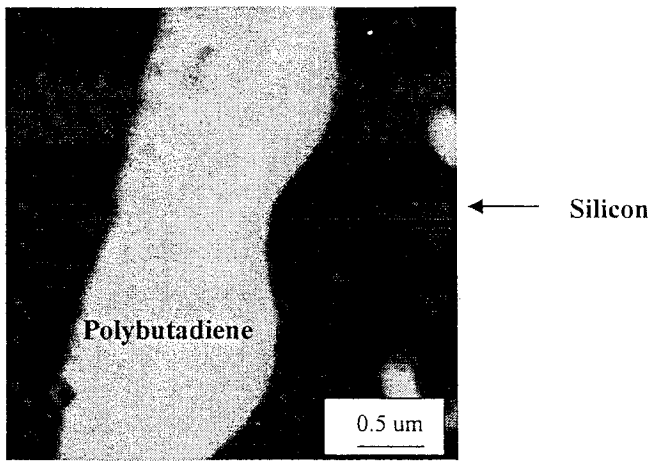

Figure 1-4 Phase image of polybutadiene film on silicon, grayscale is 0-40° from black to white

1.3 The influence of material properties on the phase image

The phase of the probe response is influenced by the forces resulting from the interaction between the tip and sample surface. The relevant interaction forces are the van der Waals force, the elastic force and the viscous force[8-13]. The tip-sample interaction forces differ for different materials and are the focus of this work. The van der Waals force is caused by an induced dipole of an electron cloud of the atoms[1-2]. Therefore it relates to the radius of the atoms in the material. The elastic force is due to the elastic deformation of material and exists when the tip is in contact with the material surface. When the tip withdraws from the surface, the elastic deformation energy is returned to the probe and causes the tip to leave the surface faster. The viscous force is caused by the friction created from the relative movement of atoms or groups of atoms. This energy is dissipated and can not be returned to the probe. Therefore, for soft, viscous materials, the

probe leaves the material surface at a slower speed than it would on an elastic material. For this reason, generally speaking, the probe has a higher phase on soft, viscoelastic materials than it does on hard, elastic materials and in the phase image soft viscoelatic regions are brighter than hard elastic regions[13-14].

Material properties also slightly influence the topography image. For soft materials, because the tip indents into the material, the tip-sample separation is smaller when the amplitude is the same. This results in a lower topography being recorded. If a soft material traps the tip or sticks to the tip, the controller has to maintain a larger separation distance to give the same amplitude, so that the apparent topography is higher than reality. All of these influences on topography remain small and are neglected in our study.

1.4 The influence of the set point on the phase image

The set point is defined as the engaged amplitude divided by the free vibration amplitude, as shown in Fig.1-5. The set point influences the phase image because it influences the tip sample interaction force. As the set point decreases, the tip-sample interaction force increases. The relation between the phase and the set point is more complicated. Generally speaking, when the set point decreases from 1.0 to 0.0 the phase is larger than 90° at first, then smaller than 90°, and finally larger than 90° again[15]. The phase change from smaller than 90° to larger than 90° is due to the change of the average force from attractive to repulsive. The change from larger than 90° to smaller than 90° at lower set point is likely due to a change in the vibration mode or to the tip becoming trapped on the surface.

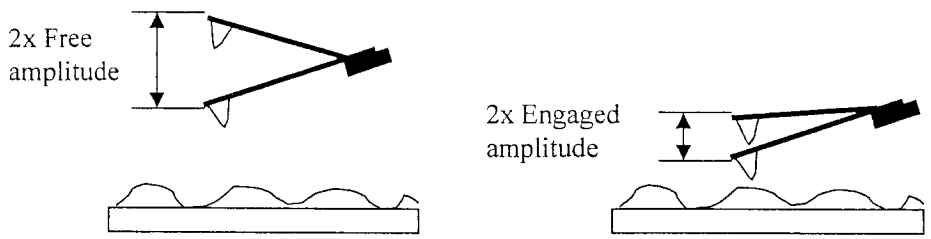

Figure 1-5 Free vibration amplitude and engaged amplitude used to define the set point ratio

1.5 Polymers and viscoelastic properties

The polymer molecule is composed of many small repeating units called "mers" or monomers. These monomers connect to each other and form a polymer chain during polymerization. For most polymers, when a stress is applied the chains will deform and there will be relative movement between different chains. When the stress is removed, only some of the deformation, called elastic deformation, can be recovered. The rest is a permanent deformation. This behavior is called viscoelastic behavior. Viscoelastic polymers also exhibit stress relaxation, meaning that when a strain is applied the internal stress will change with time due to the relative movement of polymer chains. When the deformation or deformation rate imposed on a viscoelastic material is small, the increase of stress and strain at a fixed time is linear and the strain caused by the stress at different times can be superposed. This is called linear viscoelastic behavior[16-17]. To describe such relaxation properties, the Maxell model is introduced in Fig. 1-6.

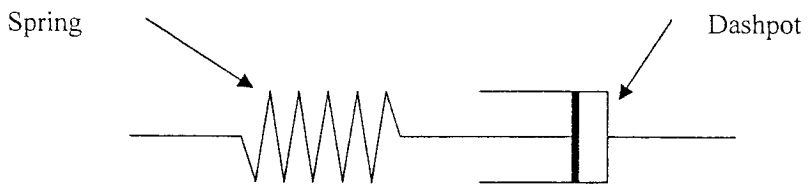

Figure 1-6 Maxell model

It is composed of a spring with an elastic modulus G and a dashpot with viscosity η. The time dependent elastic modulus for this element is:

$$G(t) = G[\exp(-t/\lambda)] \qquad [1.1]$$

where $\lambda = \eta / G$. Because polymers have many chains with different lengths and the chains entangle with each other forming many sections, the relaxation properties are more complicated than a single Maxell element. Here a generalized version of the Maxell model can be useful:

$$G(t) = \sum_{i=1}^{N} G_i[\exp(-t/\lambda_i)] + G_e \qquad [1.2]$$

where G_e is the equilibrium modulus

In tapping mode AFM, when the tip touches the sample surface, only some of the monomers in the polymer chain are involved in the movement and the number of monomers involved changes with the indentation depth. Therefore we need to know the

viscoelastic properties on the monomer scale. Moreover, because the contact time of the tip and sample is short, we need the material properties at a very short time scale. The experimental technique for measuring these properties is the small-amplitude oscillatory shear (SAOS) test.[16] SAOS is a rheological experiment designed to characterize complex fluids. In this experiment, the material is placed between two parallel plates or a cone and plate, and subjected to a periodic shear-rate. The stress response of the material is detected and used to calculate the storage modulus and the loss modulus. The shear strain and stress response of the SAOS test is given by

$$\gamma_{21} = \gamma_0 \sin \omega t \qquad [1.3]$$

$$-\tau_{21} = \tau_0 \sin(\omega t + \alpha) \qquad [1.4]$$

where γ_{21} and γ_0 are the shear strain and shear strain amplitude. The τ_{21}, ω, and α are shear stress, angular frequency and phase angle respectively. The storage modulus and the loss modulus can be calculated by

$$G' = \frac{\tau_0}{\gamma_0} \cos \alpha \qquad [1.5]$$

$$G'' = \frac{\tau_0}{\gamma_0} \sin \alpha \qquad [1.6]$$

With the storage and loss modulus we can calculate the complex viscosity:

$$\left|\eta^*\right| = \sqrt{\left(\frac{G'}{\omega}\right)^2 + \left(\frac{G''}{\omega}\right)^2} \qquad [1.7]$$

The Cox-MERZ relationship is:

$$\eta(\dot{\gamma}) = \left|\eta^*\right|_{\dot{\gamma}=\omega} \qquad [1.8]$$

With this we can estimate the shear viscosity of materials. Because of the frequency limit of the instruments, the material properties obtained from the SAOS test do not cover the monomer relaxation time scale. Therefore, it is necessary to perform time-temperature superposition to find material properties in the small time region. If the viscosity curve at different temperatures has the same shape, the viscosity curve measured at a high temperature can be shifted to the lower temperature and the viscosity at the small time scale is obtained.

2. Overview of previous work

Many works have been done to study the influence of material properties on AFM images. [3-15] The main purpose of those works are usually to use the AFM image to extract the information about the material properties. The topography influence on the phase image has been proven to be small,[15] so most of the previous works focus on the influence of mechanical properties on the phase image. There are two methods used to evaluate the influence of mechanical properties on the phase image: the direct simulation method and the energy method. [1] The direct simulation method involves establishing the probe vibration model and the probe-sample interaction model and using numerical simulations to find the phase of the probe response. The energy method also requires the establishment of a model that is similar to the numerical simulation method; however, this method uses the energy conservation law to find the relationship between the phase and other parameters. For both methods, the first step is to establish a vibration model and a probe-sample interaction force model.

2.1 The vibration model

The AFM probe is composed of the tip and the cantilever. When it vibrates, the cantilever deflects like a spring. The damping from the air and inside probe can be treated as a dash pot with the damping coefficient c. So the probe vibrating in the air behaves as a single point-mass vibration system shown as Fig. 2-1.[18-24] The spring constant is k, the activation force is $F_0 \sin \omega t$ which comes from the piezoelectric material at the end of the

cantilever. The effective mass[15] is $m = k / \omega_0^2$, where ω_0 is the resonance frequency of the probe.

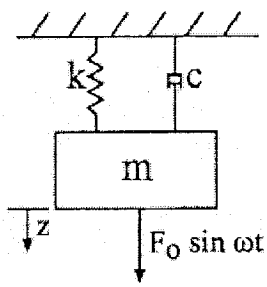

Figure 2-1 Vibration system of tip-cantilever assembly[15]

When the tip is far from the sample surface, there are no tip-sample interaction forces. In that case the probe vibration can be described by[15]:

$$m\frac{d^2z}{dt^2} + c\frac{dz}{dt} + kz = F_0 \sin \omega t \qquad [2.1]$$

where z is the instantaneous tip position relative to the static equilibrium position. Eq. 2.1 can also be written as

$$m\frac{d^2z}{dt^2} + \frac{m\omega_0}{Q}\frac{dz}{dt} + kz = F_0 \sin \omega t \qquad [2.2]$$

where Q is the quality factor and ω_0 is the free resonance frequency. When the tip touches the sample surface the probe vibration can be described by

$$m\frac{d^2z}{dt^2} + c\frac{dz}{dt} + kz = F_0 \sin \omega t + F_{ts} \qquad [2.3]$$

where F_{ts} is the tip-sample interaction force.

2.2 Model of the tip-sample interaction force

The tip-sample interaction force can be divided into the van der Waals force, the elastic force and the viscous force. Some models of these forces are established by previous work as we will discuss now.

2.2.1 Van der Waals forces

The van der waals force is caused by atomic dipoles [2]. The attractive force between two atoms is described by the van der Waals potential [1]:

$$w(r) = -C / r^6 \qquad [2.4]$$

where r is the distance between the two atoms and C is the interaction constant determined by polarizability and dipole moments of the atoms. The interaction force between the macroscopic tip and the macroscopic surface is the sum of interaction forces between the atoms on both the tip and the sample surface. The tip-sample system can be considered as a sphere-surface geometry. For this geometry, the interaction energy is

$$W(D) = -HR / 6D \qquad [2.5]$$

where D and H are tip-sample distance and the Hamaker constant and R is the tip radius. The van der Waals force between the tip and the sample surface is obtained by

$$F_{van} = dW(D) / dD = HR / 6D^2 \qquad [2.6]$$

To establish a model describing the probe vibration and the tip-sample interaction, one must create a coordinate that describes the relative position of the tip and sample, the instantaneous position of the tip, and the equilibrium position of the tip. This coordinate is shown in Fig. 2-2.

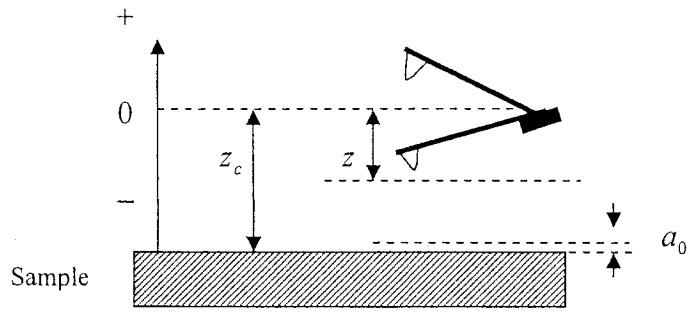

Figure 2-2 Schematic of the cantilever-tip and the sample showing the coordinate z

Then the Eq.2.6 can be written as

$$F_{van} = -\frac{HR}{6(z_c + z)^2} \qquad z_c + z > a_0 \qquad [2.7]$$

where z_c is the tip-surface separation and is a positive number , z is the tip position relative to the equilibrium position, and a_0 is the interatomic distance. When $z_c + z \le a_0$, the tip contacts the surface, and $z_c + z$ in the denominator of Eq.2.7 is replaced by a_0, because the distance between the atoms of the tip and the sample cannot be made any smaller than a_0 [15]. In this situation, the van der Waals force is often calculated using contact force models as shown in the following sections.

2.2.2 Elastic force

When the tip is in contact with the sample surface, the tip-sample interaction forces will include the elastic force, the viscous force, and the van der Waals force. The elastic force and the van der Waals force are often included in one model. The Johnson-Kendall-Roberts (JKR) and the Derjaguin-Muller-Toporov (DMT) models are the most common examples [1]. The van der Waals force is also called the "adhesion" force in these

models to distinguish them from the van der Waals force when the tip does not touch the surface. (Eq.2-7)

2.2.2.1 The DMT model[1]

In the DMT model the elastic force is given by

$$F_{DMT}(z_c, z) = \frac{4E^* R^{1/2}}{3 - 3v_s^{\ 2}}(a_0 - z - z_c)^{3/2} \qquad [2.8]$$

$$\frac{1}{E^*} = \frac{1 - v_t^{\ 2}}{E_t} + \frac{1 - v_s^{\ 2}}{E_s} \qquad [2.9]$$

where E_t, E_s and E^* are Young's modulus of the tip, sample and tip-sample contact, v_s and v_t are the Poisson's coefficients of the sample and the tip respectively. The adhesion force or contact van der Waals force, is given by

$$F_a = 4\pi R\gamma = \frac{3}{2}\frac{HR}{6a_0^{\ 2}} \qquad [2.10]$$

where γ is the surface energy.

2.2.2.2 JKR model[1]

For the JKR model, the normalized penetration of the tip is given by a function of the applied force:

$$\bar{\delta} = \frac{\delta}{\delta_a} = 3\left(\bar{F}_{JKR} + 2 + 2\sqrt{1 + \bar{F}_{JKR}}\right)^{2/3} - 4\left(\bar{F}_{JKR} + 2 + 2\sqrt{1 + \bar{F}_{JKR}}\right)^{1/6} \qquad [2.11]$$

$$\delta_a = \left(\frac{\pi^2 R\gamma^2}{3E^*}\right)^{1/3} \qquad [2.12]$$

$$\bar{F}_{JKR} = \frac{F_{JKR}}{F_a} \qquad [2.13]$$

$$\delta = a_0 - z - z_c \qquad [2.14]$$

where δ is the penetration depth of the tip and F_{JKR} is the elastic force of the JKR model. In this model the adhesion force is given by:

$$F_a = 3\pi R\gamma = \frac{9}{8}\frac{HR}{6a_0^2} \qquad [2.15]$$

2.2.3 Viscous force

When the tip indents into viscoelastic polymers, beside the elastic force due to the elastic deformation of the molecular chain, there is also a force related to the friction of the relative movement of the monomers. Scott et al. [15]proposed that this force is mainly related to the viscous properties of the material and is given by

$$F_{vis} = \eta V_t \sqrt{R\delta} = \eta V_t \sqrt{R(a_0 - z - z_c)} \qquad [2.16]$$

where η is the viscosity of material, V_t is the tip velocity. R and δ are tip radius and indentation depth. They suggested that F_{vis} is proportional to the surface area ($\propto R(a_0 - z - z_c)$) divided by the distance (perpendicular to the surface) of the material influenced by the tip. But because this distance is hard to quantify, they use $\sqrt{R(a_0 - z - z_c}$ in the model to obtain the correct order of magnitude.

Tamayo and Garcia[20] proposed a viscous force model

$$F_{vis} = \eta\frac{d\varepsilon}{dt} = \frac{\pi\eta R}{h}(a_0 - z - z_c)\frac{dz}{dt} \qquad [2.17]$$

where dz/dt is the tip velocity and h is the thickness of the sample. Because h can be quantified, they do not need to use the square root to correct the order of magnitude.

Dubourg et al. [23-24] started from the Navier-Stokes equation to analyze the viscous force. The Navier-Stokes equation is given by

$$\rho\frac{\partial v}{\partial t}+\rho(v\nabla)v=-\nabla p+\eta\Delta v \qquad [2.18]$$

Where ρ is the liquid density, p the pressure and the v instantaneous velocity of the fluid. The Reynolds number is given by

$$R_e=\frac{\rho v\Phi}{\eta} \qquad [2.19]$$

where Φ is the characteristic length of the solid. If the Reynolds number is small, the inertial term $\rho(v\nabla)v$ is negligible compared to the viscous term $\eta\Delta v$.

Dubourg et al. show that for the AFM, where the amplitude, $A=10^{-8}$ m, $\omega=10^{6}$ rad/s, $\rho=10^{3}$ kg/m, and the tip velocity is equal to the fluid velocity, the Reynolds number is $R_e\cong10^{-7}$.They also evaluated the stationary behavior by

$$R_{ns}=\frac{\rho\dfrac{\partial V_t}{\partial t}}{\eta\Delta V_t}=\frac{\rho\omega\Phi^2}{\eta} \qquad [2.20]$$

For the AFM, they found $R_{ns}=10^{-7}$. Both R_e and R_{ns} are small, so the viscous force is dominant in the Navier-Stokes equation. Then, in the case of a simple liquid, when the indentation depth is much smaller than the tip radius, the viscous force is given by:

$$F_{vis}=3\pi\eta\delta V_t \qquad [2.21]$$

where the parameters are the same as Eq.2.16. For polymer melts, they suggest that η may vary as the tip indents the surface because more monomers are involved in the movement. The viscosity can then be calculated by

$$\eta\sim\eta_m\frac{\psi^2}{a^2} \qquad [2.22]$$

where $\psi \cong \sqrt{R\delta}$ is the diameter of the contact area between the tip and the polymer, a the monomer length and η_m the monomer viscosity. To use this relation, the tip-sample contact time must be larger than the monomer relaxation time. Finally the viscosity force is given by

$$F_{vis} = 3\pi\eta_m R\left(\frac{\delta}{a}\right)^2 V_t \qquad [2.23]$$

2.3 Set point influence on phase image of AFM

The set point strongly influences the phase image of the AFM because it influences the tip-sample interaction force. These influences produce a combined effect with the material influences. Therefore this factor needs to be considered in both the numerical simulation method and the energy method. A typical curve of the set point influence on phase angle for one material is shown in Fig.2-3. Here, the Y axis is not the phase of the probe response but the phase angle, which is equal to 90° minus the phase of the probe[15].

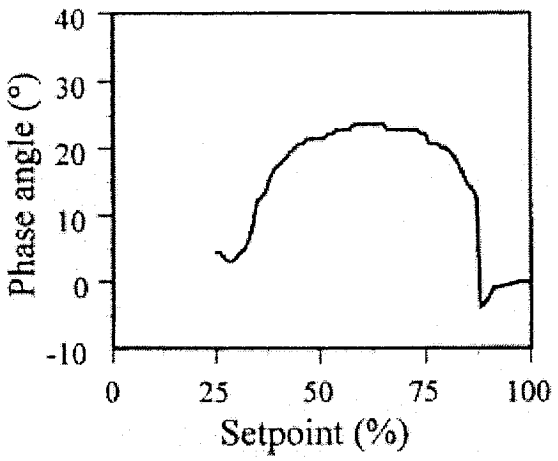

Figure 2-3 The phase angle at different set point for free amplitude 190mm and Si (100)[15]

In the Fig.2-3, when the set point is larger than 0.85, the phase angle is negative meaning that the phase is bigger than 90°. The reason for this is that the tip only touches the surface a little, the dominant force of the tip-sample interaction is the van der Waals force, and the average force is attractive. When the set point is between 0.6 and 0.85, the dominant force of the tip-sample interaction is the viscous force or the elastic force, and the phase angle is positive meaning the phase is smaller than the 90°. When the set point is smaller than 0.60, the phase angle begins to decrease and finally becomes negative again. This is probably due to the deep indents which occur in soft materials at low set points, causing the tip to be trapped in the material and resulting in a phase reversal. This phenomenon does not occur for all materials.

2.4 Influence of material properties on the phase image of AFM

2.4.1 Direct simulation method

Many previous works have used numerical methods to study the influence of mechanical properties on the phase image. [15, 20, 21] In this method one needs to combine the force models and the vibration models that were previously explained. Garcia et al. [21] studied the phase at different set points and different frequencies using the following model, which includes the DMT model for F_{ts}.

$$m\frac{d^2z}{dt^2}+\frac{m\omega_0}{Q}\frac{dz}{dt}+kz=F_0\sin\omega t-\frac{HR}{6a_0^{\ 2}}+\frac{4E^*R^{1/2}}{3-3\nu_s^{\ 2}}(a_0-z-z_c)^{3/2} \qquad [2.24]$$

Their simulation results in Fig. 2-4 show the phase reversal when normalized separation z_c / A_0 decreases where A_0 is the free vibration amplitude, . This is due to the average force changing from an attractive force to a repulsive force.

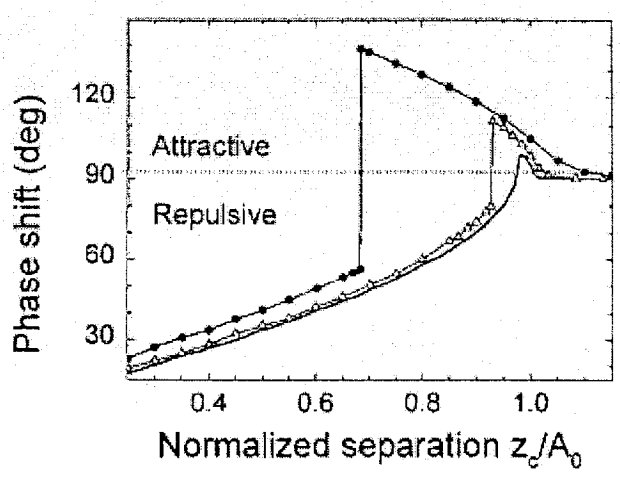

Figure 2-4 Phase-shift dependence on normalized tip-sample separation. Solid line with dark dot symbols is for 10 nm amplitude, hollow triangle symbols for 30 nm amplitude and solid line only for 60 nm amplitude [21].

Their experimental data in Fig.2.5 show that compliant materials (such as polyethylene) have the largest percent of attractive regime (the set point range influenced by the attractive force) and that the attractive regime always decreases as free amplitude increases[21]. Therefore a large free amplitude can diminish the influence of the attractive forces and shrink the negative phase angle region. That is the reason why it is difficult to observe the negative phase region with a large free amplitude.

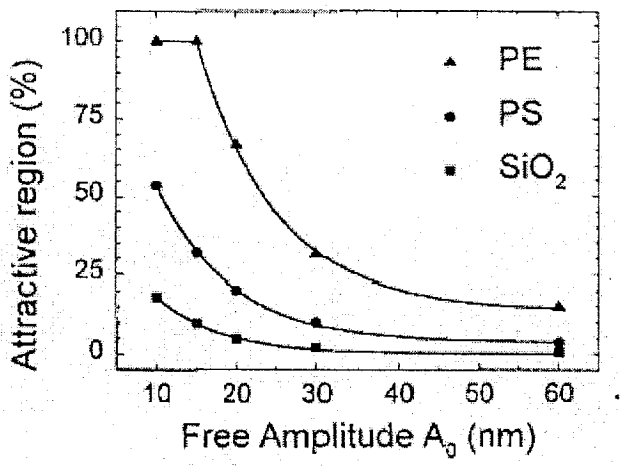

Figure 2-5 Attractive regimes for different materials (compliant polyethylene (PE), intermediate polystyrene (PS), and stiff SiO_2) [21]

Tamayo and Garcia[20] studied the deformation, contact time and phase contrast for different materials using the following model

$$m\frac{d^2z}{dt^2}+\frac{m\omega_0}{Q}\frac{dz}{dt}+kz=F_0\sin\omega t-\frac{HR}{6a_0^{\,2}}+\frac{4E^*R^{1/2}}{3-3\nu_s^{\,2}}(a_0-z-z_c)^{3/2}+\frac{\pi\eta R}{h}(a_0-z-z_c)\frac{dz}{dt}$$

[2.25]

Their simulation results in Fig. 2-6 show that if the elastic modulus is the same, materials with higher viscosity will display a larger phase shift (phase lag). For elastic materials, a larger elastic modulus results in a smaller phase shift. Fig. 2-6 also shows that the effect of material properties on the phase shift increases as the tip-sample separation distance decreases.

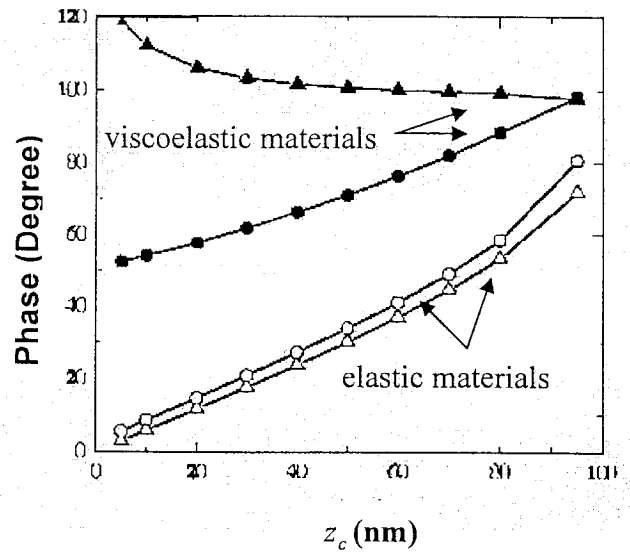

Figure 2-6 Simulated results of the phase as a function of tip-sample separation distance for different samples (open triangles, elastic sample E=70 GPa; open circles, elastic sample E=0.3 GPa, filled circles, viscoelastic sample E=0.1GPa, η=30 Pa.s; filled triangles, viscoelastic sample E=0.1 GPa, η=400 Pa.s)[20]

Scott and Bhushan[15] studied the influence of viscosity on the phase angle for a silicon surface. The model they used is:

$$m\frac{d^2z}{dt^2}+\frac{m\omega_0}{Q}\frac{dz}{dt}+kz=F_0\sin\omega t-\frac{HR}{6a_0^{\,2}}+\frac{4E^*R^{1/2}}{3-3v_s^{\,2}}(a_0-z-z_c)^{3/2}-\eta\sqrt{R(a_0-z-z_c)}\frac{dz}{dt}$$

[2.26]

Their simulation results in Fig. 2-7 show that the phase angle difference is not significantly affected by the viscosity. This is because the elastic force is the dominant force for stiff silicon, and the viscous force influence is much smaller. They did not use this model to study polymers.

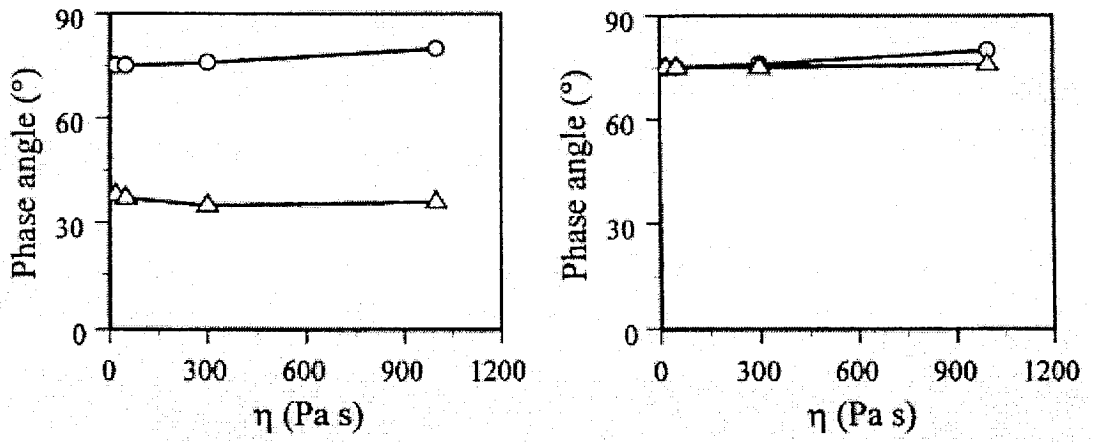

Figure 2-7 Phase angle vs. viscosity for Si(110). (a) Same free amplitude 190 nm, set point 0.4, open circles, and 0.9, open triangles. (b) Same set point 40%, free amplitude 190 nm, open circle, and 75 nm, open triangle[15]

2.4.2 The energy method

The energy method has also been used by many researchers. Cleveland et al [1,25]assumed that the energy input to the cantilever must be equal to the energy dissipated in the environment and on the sample surface.

$$E_{ext} = E_{med} + E_{dis} \qquad [2.27]$$

E_{ext} is the energy from the exciting force, E_{med} the energy dissipated in the environment, E_{dis} the energy dissipated on the sample surface. They are given by

$$E_{ext} = \oint F_0 \cos \omega t \frac{dz}{dt} dt \qquad [2.28]$$

$$E_{med} = \oint -\frac{m\omega_0}{Q} \frac{dz}{dt} dz \qquad [2.29]$$

$$E_{dis} = \oint F_{ts} \frac{dz}{dt} dt \qquad [2.30]$$

where F_0 is the exciting force , $\oint$ the closed integral over a vibration cycle. With the assumption of the sinusoidal cantilever response $z = \cos(\omega t - \phi)$, the sine value of the phase is given by [1,25]

$$\sin\phi = \frac{\omega}{\omega_0} \frac{A(\omega)}{A_0} + \frac{QE_{dis}}{\pi k A_0 A(\omega)} \qquad [2.31]$$

where A and A_0 are the set point amplitude and free vibration amplitude.

Dubourg et al. [24] proposed a model to calculate the phase of probe response using the same principle as in Eq. [2.31]:

$$-\phi = \arcsin\left\{-u\frac{A(\omega)}{A_0}\left(1+\frac{c_{visc}}{c_0}+\frac{c_{NC}}{c_0}\right)\right\} \qquad [2.32]$$

where $u = \omega/\omega_0$ and the damping coefficient of the oscillator in the air c_0, is $c_0 = m\omega_0/Q$. The parameters c_{visc} and c_{NC} are the additional damping coefficients related to the viscous and van der Waals forces between the tip and the sample. For a spherical tip of radius R

$$c_{NC} = \frac{1}{\pi k_s \omega_0}\left(\frac{HR}{6}\right)^2 \frac{1}{z_c^4}\frac{1}{A^2}\left(1-\exp\left(-\frac{\tau_{res}k_s}{\eta_m a}\right)\right) \qquad [2.33]$$

$$k_s = E_s \psi \qquad [2.34]$$

$$\tau_{res} \approx \left(\frac{T}{\pi}\right)\sqrt{\frac{2z_c}{A}} \qquad [2.35]$$

where τ_{res} is the time during which the tip interacts with the sample.

If the viscous force is linearly dependent on a constant viscosity as in Eq.[2.21] then the viscous damping coefficient is:

$$c_{visc} = \eta\left(\sqrt{\frac{A^2 - z_c^{\,2}}{A^2}}\left(\frac{z_c^{\,2}}{A} + 2A\right) - 3z_c \arccos\left(\frac{z_c}{A}\right)\right) \qquad [2.36]$$

where $z_c = A - \delta$. If the viscosity is not constant and is described by [2.23] then it is:

$$c_{visc} = \frac{\eta}{5a^2}\left(-\sqrt{\frac{A^2 - z_c^{\,2}}{A^2}}\left(16A^3 + 130Az_cR + 83Az_c^{\,2} + 6\frac{z_c^{\,4}}{A} + 20z_c^{\,3}\frac{R}{A}\right) + 15\arccos(z_c)\left(8Rz_c^{\,2} + 4z_c^{\,3} + 2A^2R + 3A^2z_c\right)\right) \qquad [2.37]$$

Fig. 2-8 and Fig. 2-9 show that the experimental results of Dubourg et al are compared to best fits of Eq. 2.36 and Eq.2.37. In these experiments a vibrating tip approaches and retracts from a sample surface. The vertical displacement of the tip is about 20 nm and the rate is 0.5 Hz. The tip fee vibration amplitude is 55 nm. The phase shown here is not the phase lag but the real phase of the detected signal. Therefore, it is the negative of the phase of the probe in this thesis.

When the tip does not touch the surface the phase is not -90°, because the author used a frequency slightly lower than the resonance frequency to make the tip vibration stable. When fitting the models, the author compensated for this little difference by shifting the fitting free vibration phase to the experimental value. Figs. 2-8 and 2-9 show that Eq. [2.36] is a better fit than Eq. [2.37]

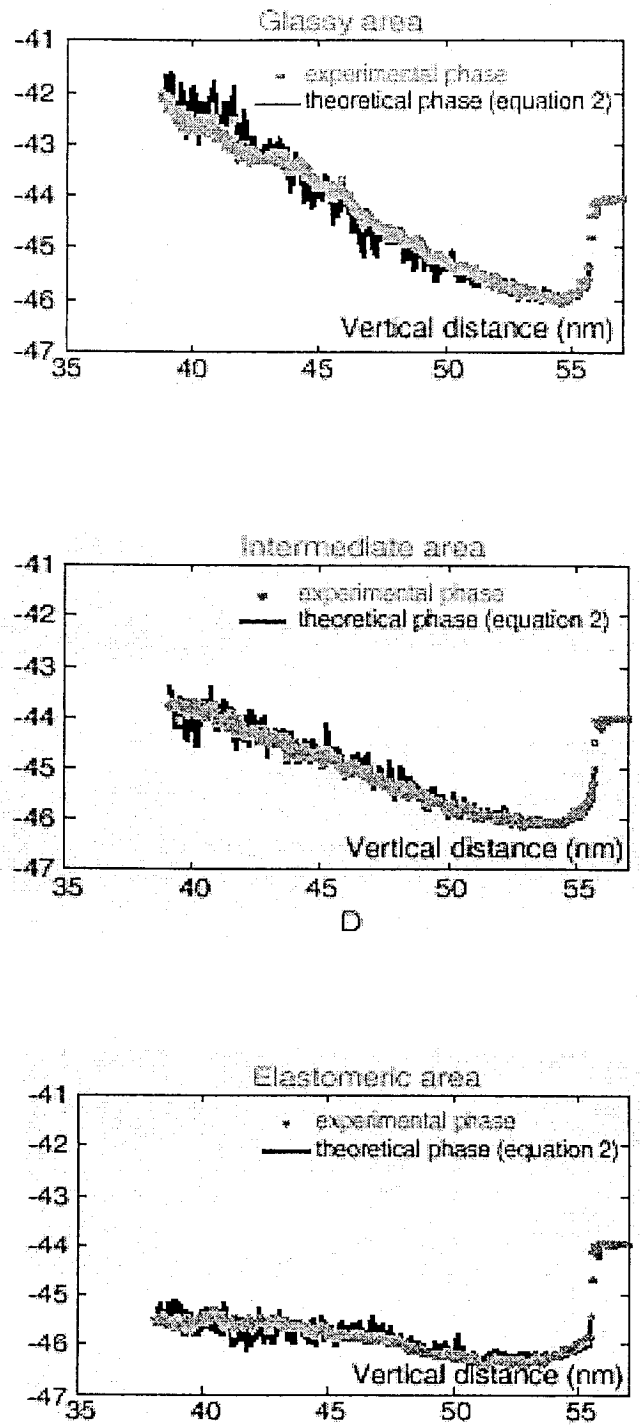

Figure2-8 Fit of the experimental data obtained on the three domains (glassy, intermediate and rubbery) using Eq. [2.36] [24].

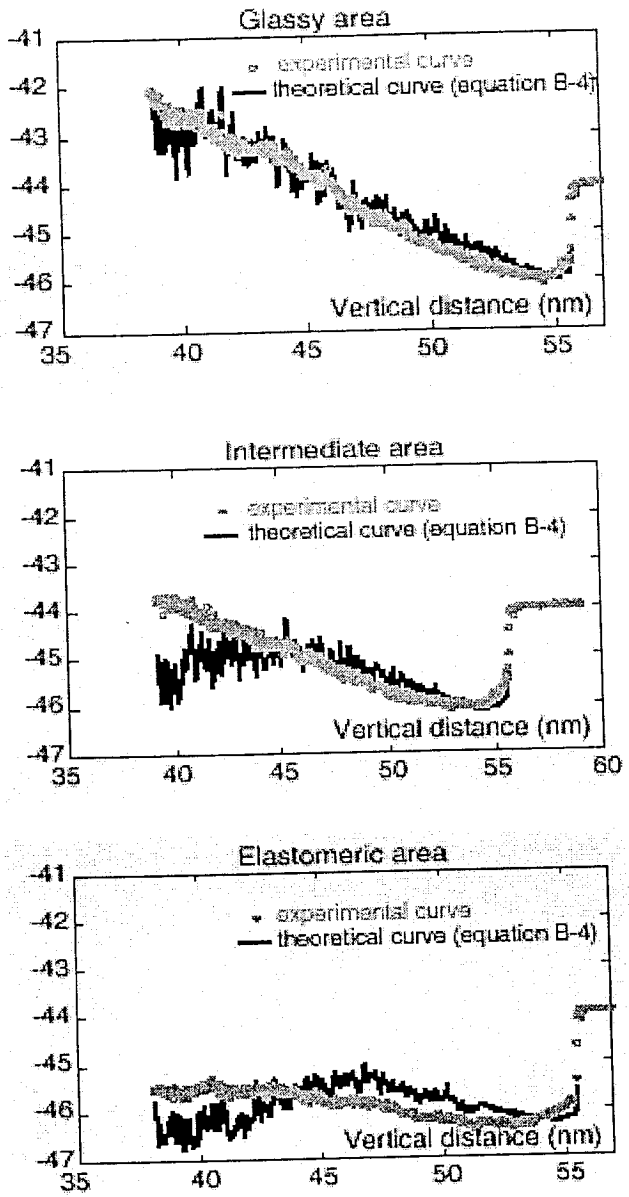

Figure 2-9 Fit of the experimental data obtained on the three domains (glassy, intermediate and rubbery) using Eq. [2.37] [24].

2.5 Topography influence on the phase image

Tamayo and Garcia proved that topography has no influence on the phase image because in their experimental images, regions of different height and size of glycerin on

graphite have the same phase shift. Scott and Bhushan[15] also found the same result in their experiments. Their image in Fig.2-10 shows that the topography image has no relation to the phase image and a surface with different topography can have the same phase shift.

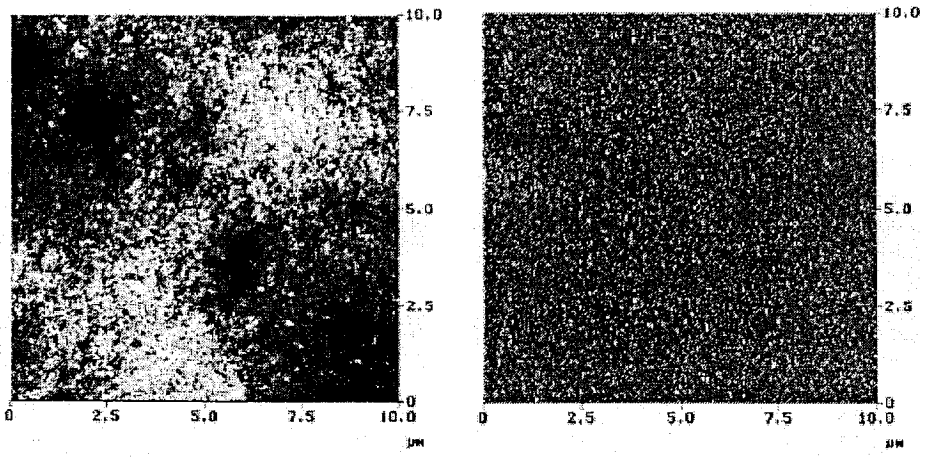

Figure 2-10 Topography and phase image of MP tape with complex magnetic layers that consist of spherical alumina particles. Grayscale is 0-150 nm for topography image and 0-90°for phase image[15].

2.6 Comment

The previous work has provided much information about the relationships of phase, the mechanical properties, and the set point. The model of Garcia et al.[21] explains the phase reversal when the set point is near 1.0 in experiments. It also shows the influence of the free vibration amplitude on the reversal region. This model however, only includes the elastic force and the van der Waals force, so it can only be used for stiff, elastic materials and it does not give the relation between phase and viscosity. The model of Tamayo and Garcia[20] includes the viscous force and it shows that the phase lag of a compliant material is higher agreeing with experiment. But, the parameter of thickness of

the polymer film in the model is not appropriate because the tip indentation only influences the polymer film near the surface. The model of Scott and Bhushan[15] has no parameter for film thickness, so it has no difficulty like this. Since their model uses the macroscale viscosity which is relatively high, the predicted tip indentation is small, and the tip-sample contact time is also short. This means that relatively small changes in viscosity have little influence, especially for stiff materials. The phase result obtained from the model of Dubourg et al. using the energy method agrees well with their experiments only when the set point is large and the tip has minimal surface contact.[24] When the tip indents deep in the material, the probe is stopped by the surface and the activation signal continues to activate the end of the probe. This energy is dissipated as a result of the friction from within the material. So the total input of energy cannot be calculated using Eq.2.28 and the energy method cannot be used in this situation. Therefore the direct simulation method seems more reasonable at smaller set points.

3. Objectives of This Work

The main objective of this work is to produce a quantitative, predictive model to describe the influence of mechanical properties on the phase image of AFM. The second objective is to use the model to simulate the TA-AFM imaging process and show the influence of mechanical properties on phase lag. The third objective is to develop a technique to infer material properties from the AFM phase image.

4. Experimental methodology

4.1 Experimental materials

Polybutadiene (PB), polystyrene (PS) and silicon (soft, intermediate and stiff) are chosen for experimental materials that are consistent with the simulation and used to test the model. Poly-l-lactic acid (PLLA) and a Polybutadiene-Polystyrene-Polybutadiene (PB-PS-PB) block copolymer are chosen to evaluate our results. PB consists of 3 types of monomers: vinyl [1,2] 8.8%, trans [1,4] 53.5 %, cis [1,4] 37.7% .Their structures are shown in Fig.4-1 where the PS monomer and PB-PS-PB structure are also shown. The PLLA structure is -[O-CH(CH3)- CO]$_n$-. The material properties are listed in Table 4-1.

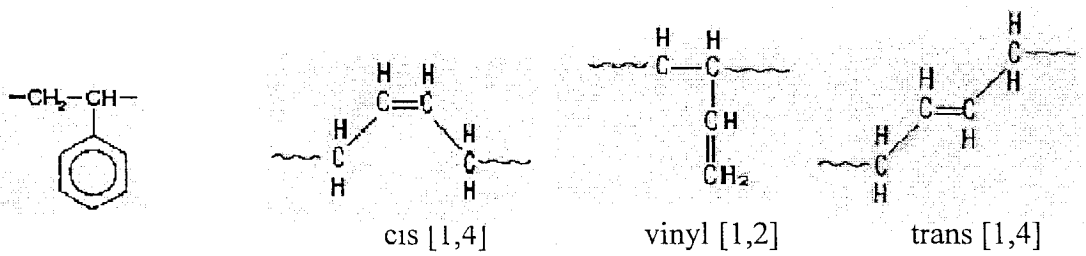

Styrene repeat unit

Butadiene repeat unit isomers

$(A\text{-}A\text{-}A\text{-}A\text{-}A)_m\text{-}(B\text{-}B\text{-}B\text{-}B\text{-}B)_n\text{-}(A\text{-}A\text{-}A\text{-}A\text{-}A)_p$-

PB-PS-PB block copolymer (A is butadiene repeat unit,
B is styrene repeat unit)

Figure 4-1 Structure of experimental materials

Table 4-1 Experimental materials

Sample	PB	PS	Silicon	PLLA	PB-PS-PB
M_W, 10^3 g/mol*	78.2	300	/	250	65-25-94
M_W/M_N**	1.04	3.0	/	1.25	1.07
E, GPa ***	/	2.92	70	3.6	/

*: M_W is the weight-average molar mass of molecule.

**: M_N is the number-average molar mass of molecule.

***: E is the elastic modulus

For the AFM experiments, it was necessary to create a surface with different material domains. To do this the polymers are separately dissolved into dichloromethane to make a 0.5 % solution and cast from a pipette on a flat silicon surface or a silicon grid surface as shown in Fig.4.2. Each sample is prepared 5 minutes before AFM imaging to avoid the generation of a layer of water on the sample surface.

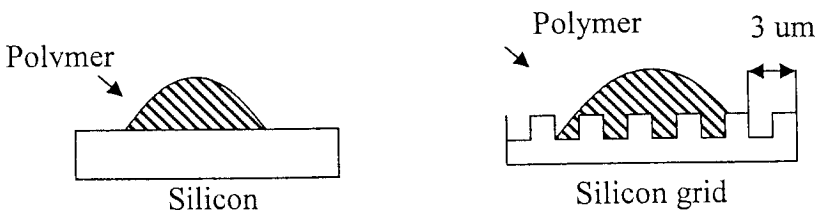

Figure 4-2 Sample for TM-AFM experiments

4.2 AFM Experiments

TM-AFM experiments were performed in an Extended Scanning Probe Microscope (SPM) of Veeco Metrology Group. The probe is a silicon rectangular cantilever with Al-coated backside. The stiffness is 40 N/m according to the manufacturer.

4.2.1 Calculation of vibration amplitude

For normal TM-AFM imaging, the free vibration amplitude is set in terms of change of voltage measured by the photodetector. The manual of the AFM also gives the reference value of the voltage. However for different probes, the same voltage represents different vibration amplitudes, because the strength and the angle of the reflected laser beam are different for each tip. Therefore, one needs to evaluate the relation between the vibration amplitude and the voltage detected by the photodetector for each probe. To do this, one must conduct experiments in the force calibration mode. Fig.4.3 shows the experimental schematic.

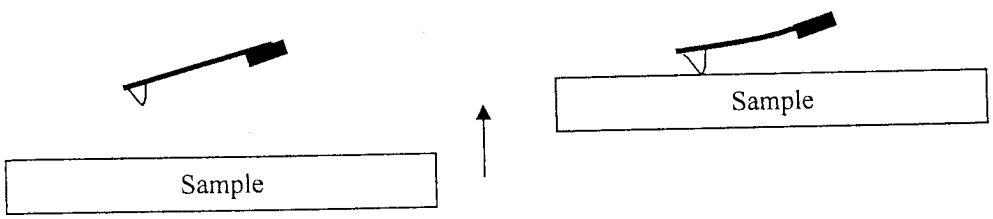

Figure 4-3 Schematic of the cantilever-tip and the sample for force calibration mode

In this schematic the probe is still and the sample moves up and down together with the scanner. When the sample touches the tip, probe deflects. If the sample is stiff, the deflection of the probe is proportional to the vertical displacement of the sample. The

voltage detected by the photodetector changes in proportion to the probe deflection. Fig 4-4 shows the experimental results.

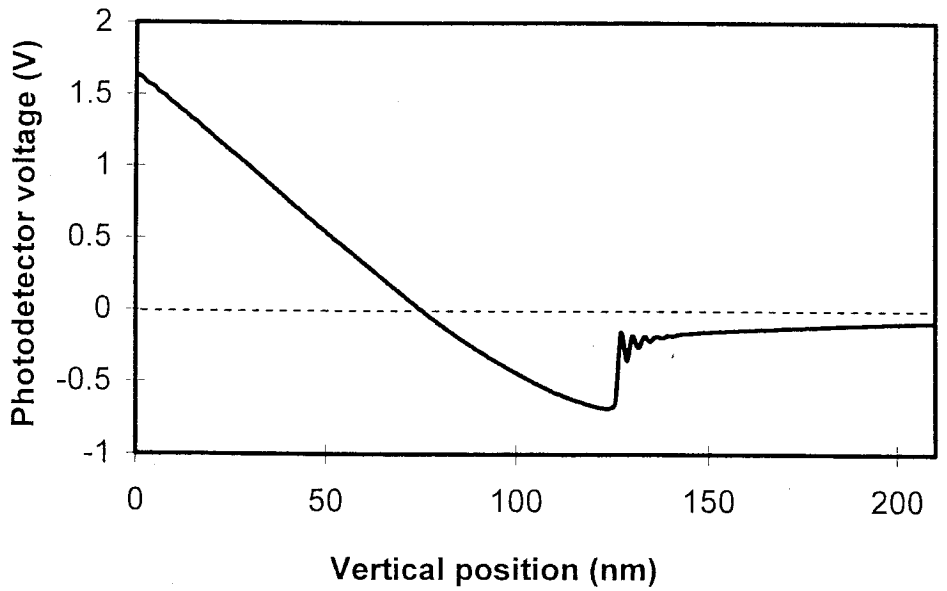

Figure 4-4 Detected voltage signal change with the sample vertical position when the tip is pulled off the silicon surface

The curve indicates that when the tip's vertical position is larger than 130 nm the tip separates from the sample and the tip deflection is about zero. When the position is between 80nm and 130 nm, the cantilever deflection is negative. This is due to the attractive van der Waals forces between the tip and the sample. When the tip position is smaller than 80 nm, the cantilever deflection is positive. This is caused by the repulsive force of the stiff surface. In this region, the tip deflection is equal to the displacement. From this curve it can be calculated that when the tip vertical displacement is about 100 nm, the voltage change in the photodetector signal is 2 V. This corresponds to an amplitude of about 50 nm for a vibrating probe. In the previous work [21], it was proven

that when the vibration amplitude is more than 75 nm the van der Waals force influence is very small. Therefore in this work an amplitude of 90 nm was used to minimize the influence of the van der Waals force.

4.2.2 Resonance frequency and quality factor

Prior to the main experiment, it is also necessary to perform a tuning experiment in order to find the resonance frequency and the quality factor of the tip. The activation signal frequency is changed from 100 KHz to 500 KHz, the frequency when the probe response amplitude is the largest is the resonance frequency. Fig. 4-5 shows that the resonance frequency is about 343.5 KHz and the vibration amplitude is about 90 nm. The phase curve is also shown in Fig. 4-5. The quality factor is automatically calculated by the AFM software (NanoScope5.12r5) from the tuning experiment data. It is given by:

$$Q_0 = \frac{\omega_0}{B} \qquad [4.1]$$

where ω_0 is the resonance frequency and B is the bandwidth of the amplitude curve at its half-power point.

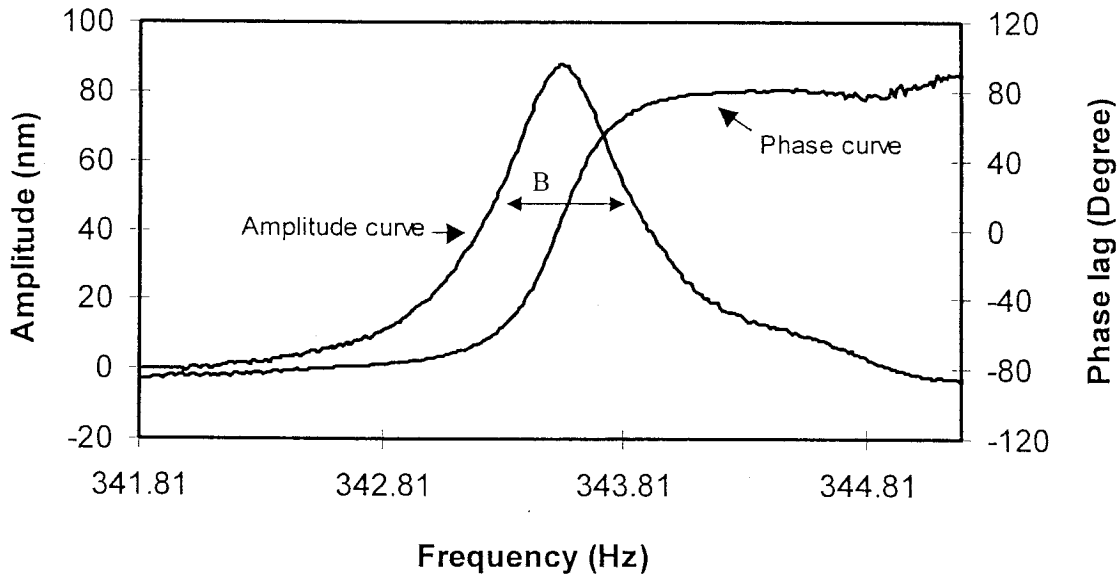

Figure 4-5 Amplitude and phase curves near the resonance frequency

4.2.3 Setting work condition

In the experiments, a very slow scan rate (0.5 Hz) is used to ensure that the tip has enough time to maintain stability on the surface. For PB on silicon, experiments were performed on two samples with different topographies. The AFM image resolution is set to 256×256 which means one image includes data from 256 scans with 256 points in each scan. For the first experiment, the Y axis movement of the probe was disabled. This ensures that the probe always scans on the same line in the x direction on the sample at different set points. For the second experiment, the probe was moved in both the X and Y directions and it scanned 256 different lines of the sample in one image. The set points were 0.9 and 0.6. Because the thickness of the PB film varies, this experimental result can be used to check the influence of the PB film thickness on the phase image.

4.2.4 Calculation of indentation depth and phase contrast

To know the indentation depth and phase contrast, it is necessary to perform a section analysis of the AFM image. Fig.4-6 shows a topography and phase image from AFM. The bright region is PB and the dark region is silicon.

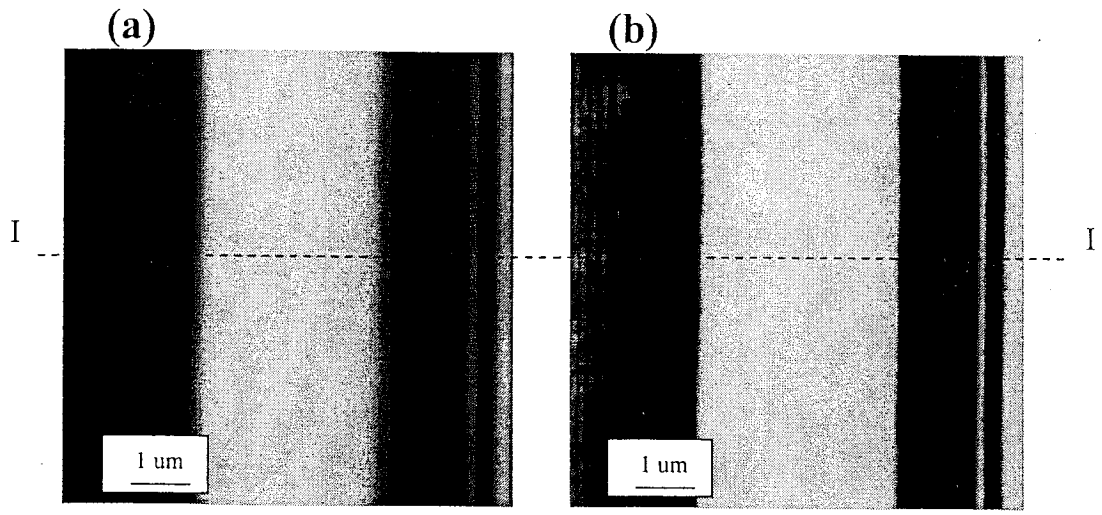

Figure 4-6 Topography image (a) and phase image (b) for PB on silicon at set point 0.6, free vibration amplitude 90nm. Grayscale is 0-150 nm for topography image and 0-50°for phase image

Fig. 4-7 and Fig. 4-8 show the section along the dashed line in Fig. 4-6. Fig. 4-7 shows that the largest apparent height of the PB film is about 104 nm at a set point 0.9 and 90 nm at a set point 0.6. This decrease of apparent height is caused by the larger tapping force and deeper indentation of the tip on the PB surface at a lower set point. Because the silicon is stiff the height change observed on silicon is essentially zero. Therefore, the indentation depth on the Polybutadiene at a set point of 0.6 is

approximately equal to the decrease of the PB height as compared to a set point of 0.9. The indentation depth here is 14 nm.

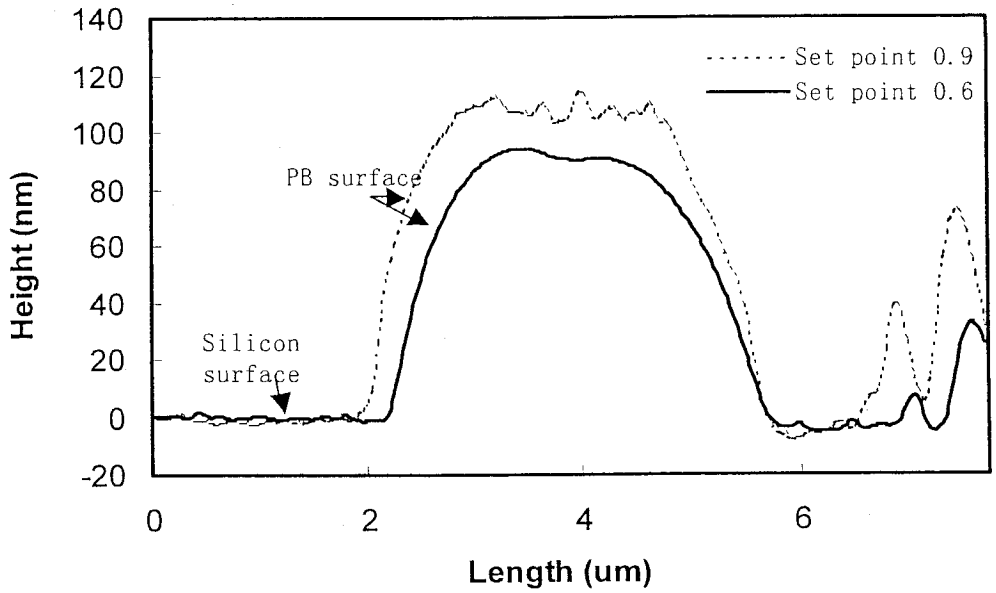

Figure 4-7 Topography section of Fig. 4-6 (a) along the line I

Fig. 4-8 shows that the phase contrast between the PB and the silicon surface is 20 degrees. These results show that section analyses of the AFM image can give us both indentation depth and phase contrast.

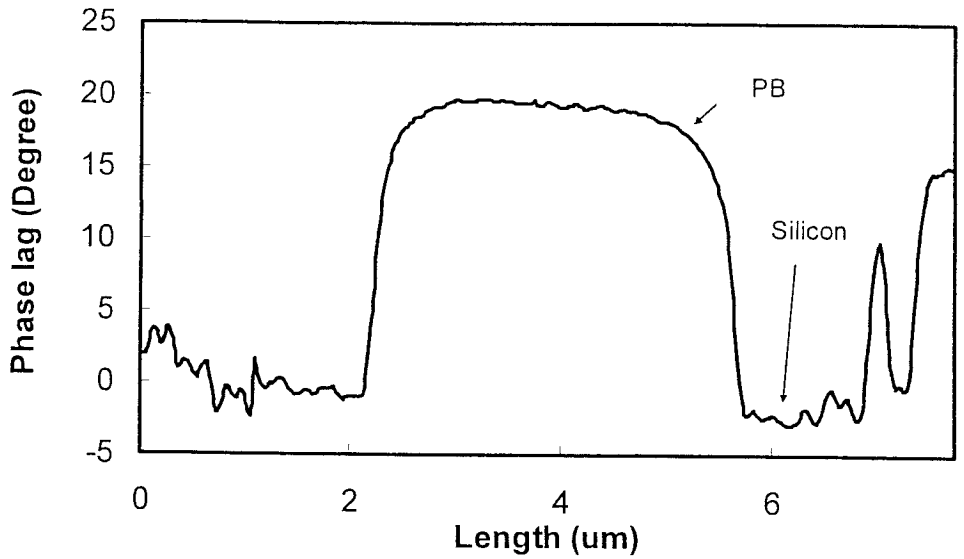

Figure 4-8 Phase section of Fig. 4-6 (b) along the line I

4.3 Oscillatory Shear Test

The oscillatory shear tests were performed by Robertson[26] in a Rheometrics ARES instrument fitted with two force rebalance transducers with maximum torques of 200 and 2000 g-cm. The main purpose of this experiment is to measure the linear viscoelastic properties of the material. The key point of the experiment is to make the test in the linear region and to ensure that the material is stable at high temperatures. In order to know if the test is in the linear region one must perform the dynamic strain or stress sweeps, obtaining complex viscosity as a function of strain (or stress). The region where the complex viscosity is constant is the linear region. To check the thermal stability one needs to do a time sweep, which means to do a test at a high temperature while maintaining constant parameters for a long period. When the complex viscosity starts to change the degradation is beginning. Fig. 4-9 shows the final test results.

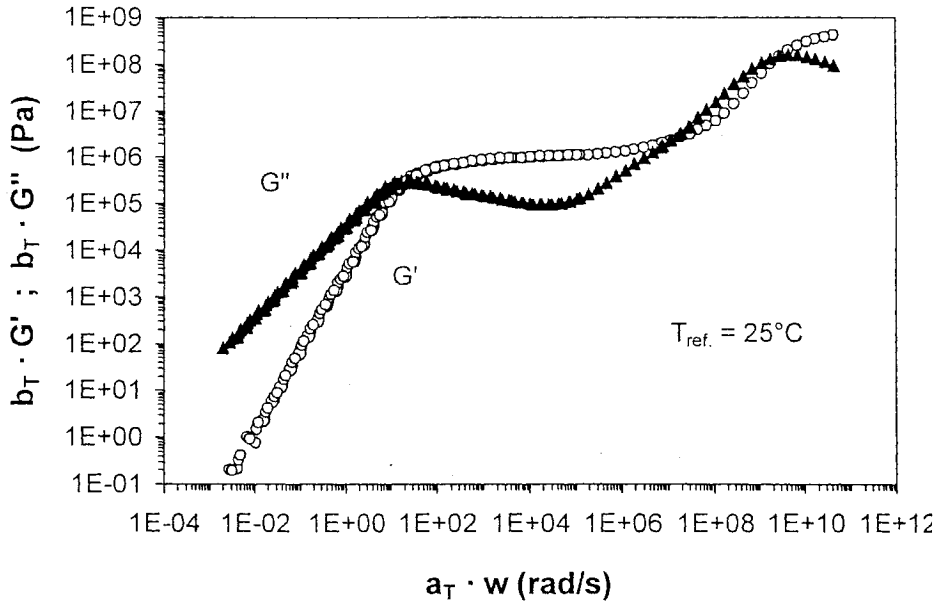

Figure 4-9 Master curve at 25 C° for PB with M_w =75000 g/mol

5. Model and simulation

5.1 Simulation model and parameters

Based on the previous work, a new model that describes both the tip vibration and the tip-sample interaction is proposed.

$$m\frac{d^2z}{dt^2}+\frac{m\omega_0}{Q}\frac{dz}{dt}+kz = F_0\sin\omega t + F_{ts} \qquad [5.1]$$

$$F_{van} = -\frac{HR}{6(z_e+z)^2} \qquad z_e+z>a_0 \qquad [5.2]$$

$$F_{ts} = -\frac{3}{2}\frac{HR}{6a_0^2}+\frac{4}{3}E^*\sqrt{R}(a_0-z-z_e)^{3/2}+3\pi R\eta_m\left(\frac{a_0-z-z_e}{a}\right)^2\frac{dz}{dt} \qquad z_e+z\le a_0 \qquad [5.3]$$

The first and second term of Eq.5-3 are from the DMT model and the third term is from the viscous force model of Dubourg et al. [24] The main difference between this model and those developed before is that the viscosity is the value at the time scale of the tip-sample contact and changes with the indentation depth during indentation. Dubourg et al. considered only the final indentation depth to determine the viscosity. To solve this model, the direct method was used because it is more reliable than the energy method at small set points. The simulation is performed in Matlab simulink using the Runge-Kutta Method. A feed back loop was put in the model to simulate the probe scanning on different materials with a constant amplitude. The simulation can give the phase contrast

between two materials as seen in the AFM imaging. Fig. 5-1 shows the structure of the feed back loop of the AFM. The whole simulation system is given in appendix 1.

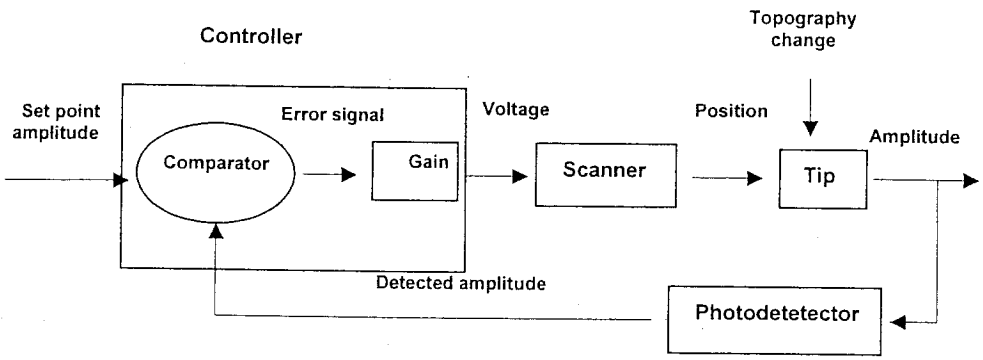

Figure 5-1 Structure of feed back loop

Simulations were performed for polybutadiene, polystyrene and silicon. Table 6-1 shows the parameters for the simulations. The quality factor Q is obtained from the tuning experiment explained in the experimental methodology section. The monomer viscosity, η_m, of PB is obtained from the oscillation test results in Fig.4-8. The oscillation cycle of the tip is about 3×10^{-6} s and the time the tip stays on the PB surface is about 10^{-7} -10^{-6} s. Therefore, the viscosity at this time scale is 0.1 Pa.s. For PS, the Young's modulus was provided by the manufacturer E_s =2.92 GPa. The corresponding viscosity is about 100 Pa.s for a time scale of 10^{-7} s, assuming $\eta = G \times t$.

Tip and cantilever					
E_t	R	Q	ω_0	k	ν_t
129 GPa	10 nm	400	$680\pi \times 10^3$ rad/s	40 N/m	0.28
Silicon surface (Silica)					
E_s		a_0		ν_s	
70 Gpa		0.234nm		0.28,	
Polybutadiene surface					
E_s	η_m		a	ν_s	
3.6×10^6 Pa	0.1 Pa.s		0.96 nm	0.5	
Polystyrene surface					
E_s	η_m		a	ν_s	
2.92×10^9 Pa	100 Pa.s		1.8 nm	0.3	

Table 5-1 Parameters for simulation

Because of the speed limitation of the computer CPU and the small time step, the simulation times is set to 1.4×10^{-3} second. It is much smaller than the real scan time of AFM for one line. This is compensated for by a large feed back gain allowing the simulated tip vibration to stabilize when it scans on various material surfaces in less than 1.4×10^{-3} s.

5.2 Simulation results for PB on silicon

Figures 5-2 to 5-4 show the simulation results when the tip free vibration amplitude is 90 nm and the set point is 0.6. When t<0.004s, the tip is not in contact with the sample surface, and Fig.5-2 shows that the tip-cantilever starts vibrating from zero amplitude to a maximum resonance amplitude of 90 nm driven by the activation force. Fig.5-3 shows that the phase lag between the tip vibration and the activating force is 90°

during this time period. Fig.5-4 shows that the tip sample separation of 92 nm is a little larger than the tip amplitude, and it therefore does not touch the surface.

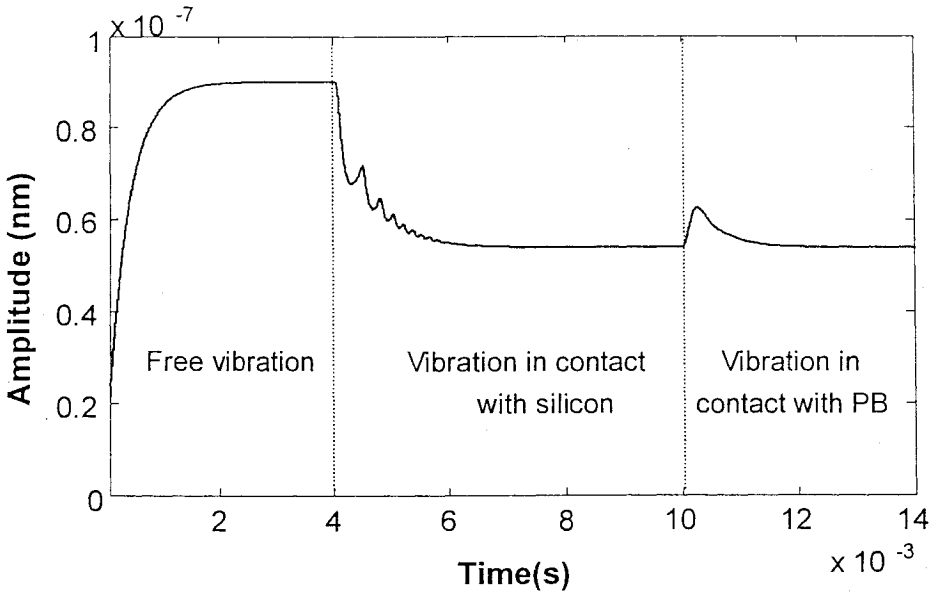

Figure 5-2 Simulated amplitude curve for PB on silicon at set point 0.6

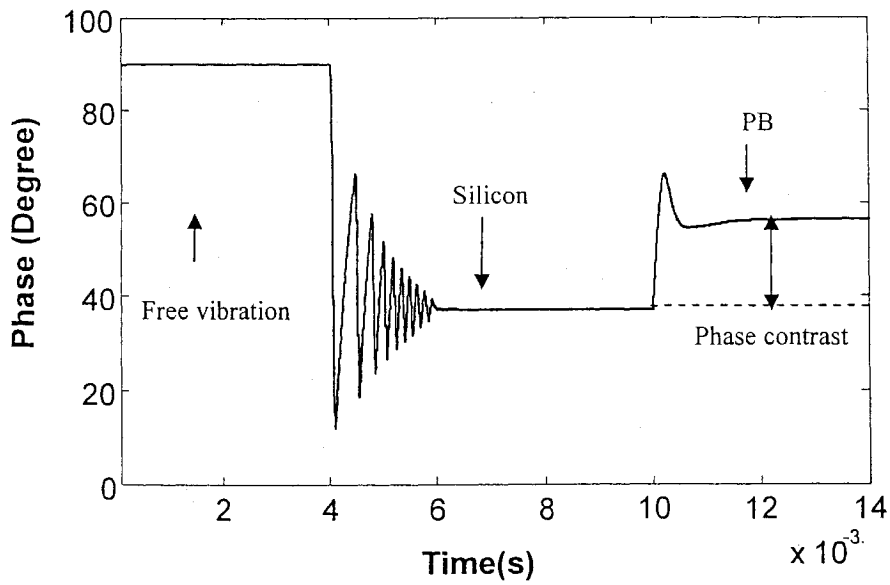

Figure 5-3 Simulated phase curve for PB on silicon at set point 0.6

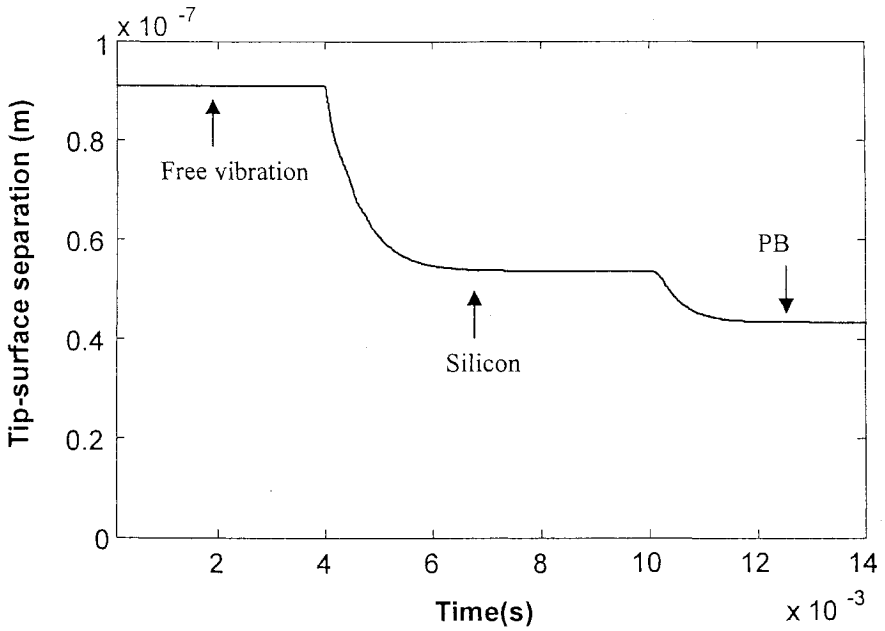

Figure 5-4 Tip-surface separation distance in the simulation for PB on silicon at set point 0.6

When 0.004s<t<0.010s, the tip approaches to the silicon surface. The contact with the silicon surface decreases the tip vibration amplitude. The feedback loop adjusts the tip-sample separation until the tip vibration amplitude arrives at the set point value of 54 nm, shown in Fig.5-2. The phase lag settles to 38° after a transient section when the feedback loop is in a state of adjustment, Fig.5-3. Fig.5-4 shows that the tip-sample separation is a 53.7 nm under this condition. This indicates that the indentation depth of the tip on the silicon surface is 0.3 nm under these conditions. It is very small and negligible.

When 0.010s<t<0.14s, the tip is in contact with the PB surface. Because the PB is soft, the amplitude increases at first, and returns to the set point value under the control of the feedback system, Fig.5-2. The phase lag increases to 58° after a short transient state, Fig.5-3, and the tip-sample separation distance decreases to 41.5 nm, Fig.5-4. The reason

for this decrease is that the indentation depth increases on the PB surface leading to an amplitude increase and the feedback loop adjusts the tip closer to the sample to force the amplitude to the set point value. The indentation depth on the PB surface is the amplitude minus the tip-separation distance. The indentation depth here is 12 nm. The phase contrast between the silicon domain and the PB domain can be determined from Fig.5-3 to be 19°.

Figs.5-5 and 5-6 show the forces acting on the tip-cantilever in one oscillation cycle when the tip is in contact with the silicon and the PB surface respectively. On the silicon, the dominant tip-sample interaction force is the elastic force, and on the PB the viscous force is dominant. It also shows that the tip-sample contact time is longer for the PB than for the silicon.

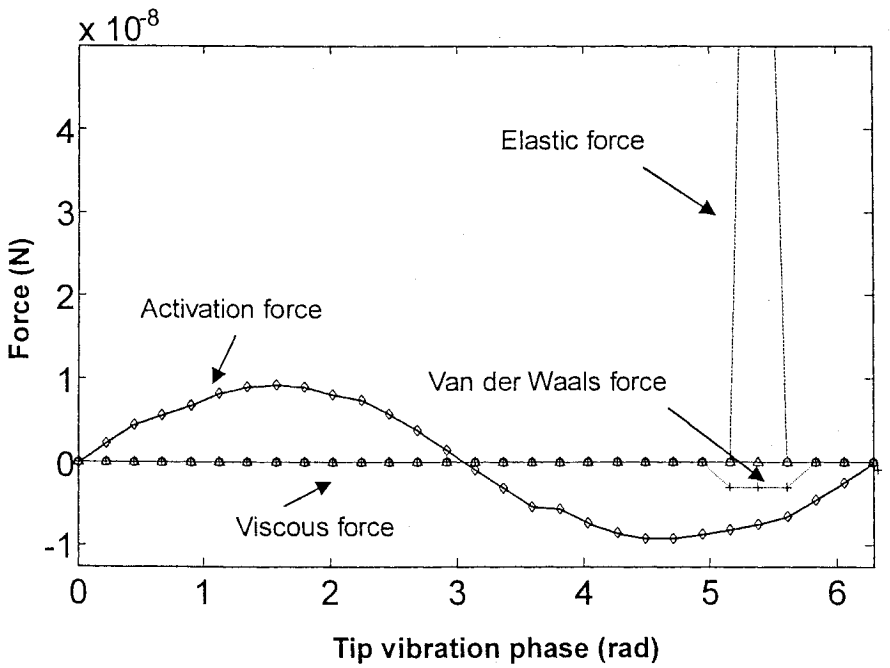

Figure 5-5 Forces acting on the tip in one vibration cycle for the silicon surface at set point 0.6

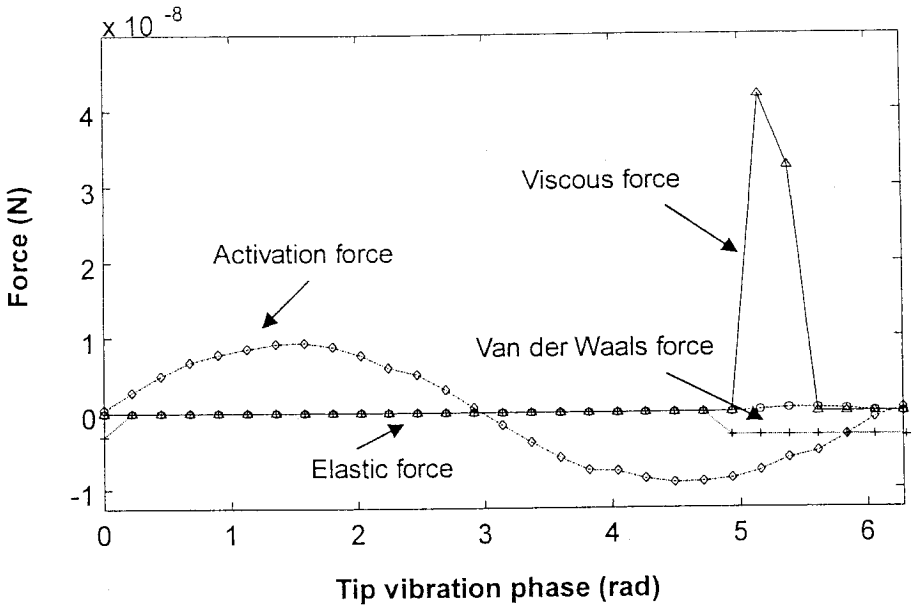

Figure 5-6 Forces acting on the tip in one vibration cycle for the PB surface at set point 0.6

The simulated indentation depth and the phase contrast at different set points are shown in Figs.5-7 and 5-8. The indentation depth increases as the set point decreases from 1.0 to 0.7. When the set point is smaller than 0.7, the indentation depth stays at 12 nm. The phase contrast between the silicon and PB surface increases as the set point decreases.

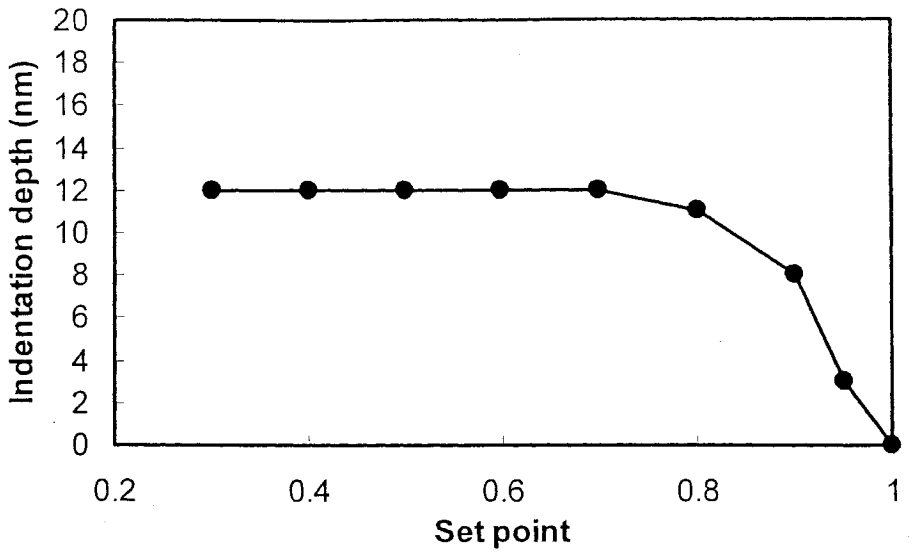

Figure 5-7 Simulated indentation depth on a PB surface

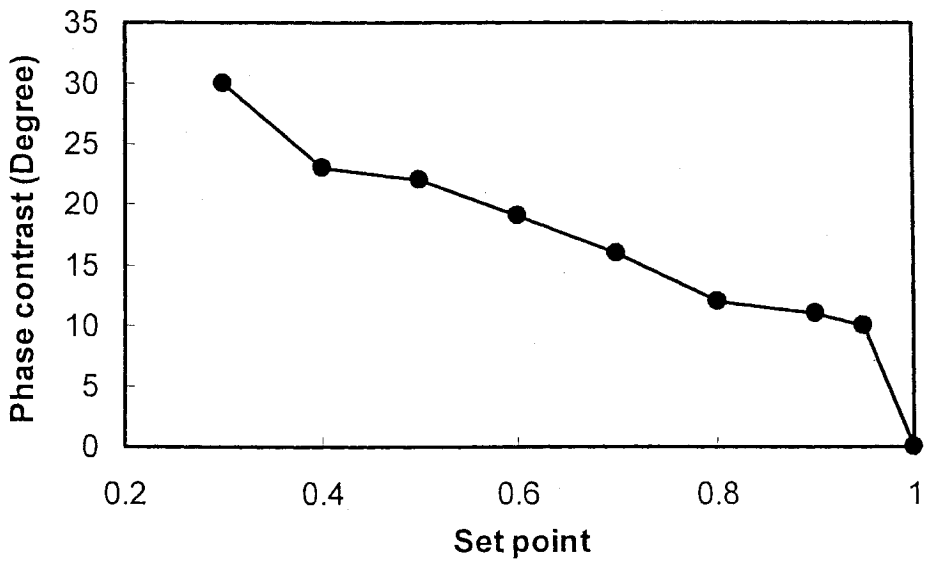

Figure 5-8 Simulated phase contrast between PB and silicon surfaces

5.3 Simulation results for PS on silicon

Figures 5-9 and 5-10 show the simulation results for PS. Because the PS is much stiffer than the PB, the indentation of the tip into the PS is very small and the phase contrast between PS and silicon is about 5 degrees.

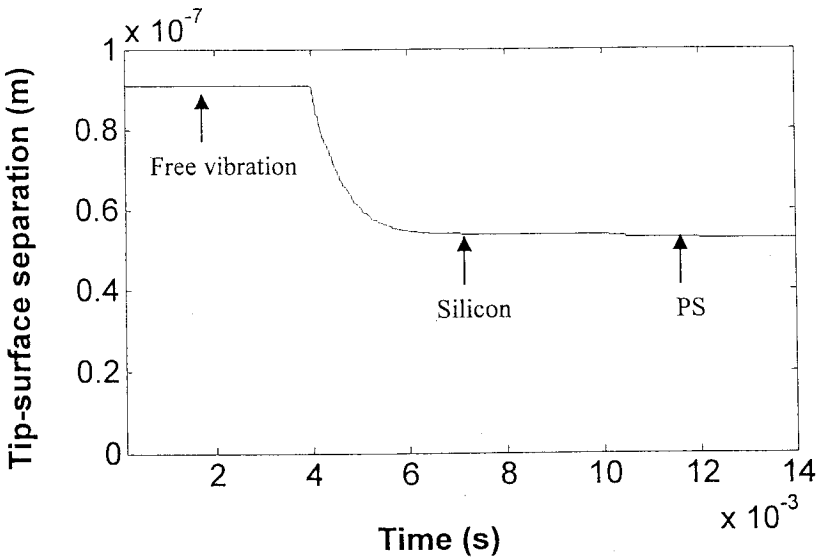

Fig.5-9 Tip-surface separation distance in the simulation for PS on silicon at set point 0.6

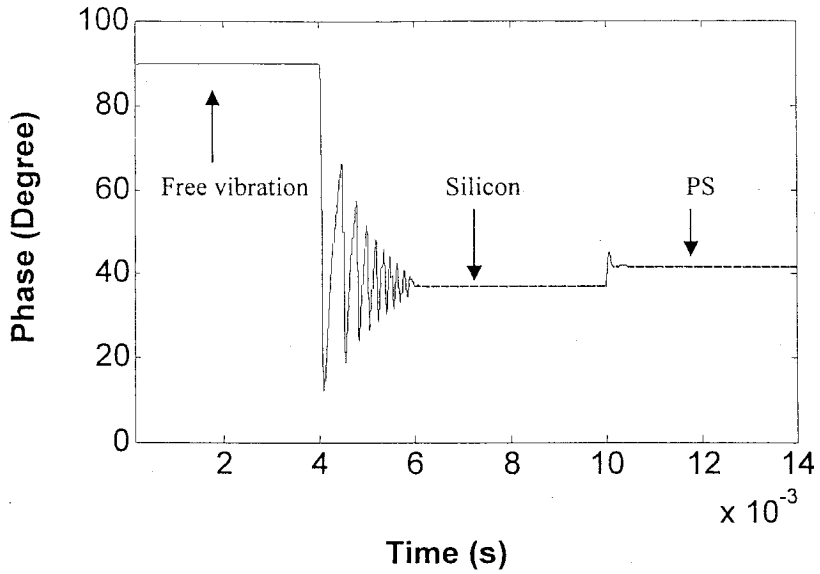

Figure 5-10 Simulated phase curve for PS on silicon at a set point of 0.6

5.4 Parametric study of viscoelastic material on silicon

Simulations were also done to look at the effect of viscosity and elastic modulus on the phase. For most polymers, the monomer length a is from 0.8 nm to 1.8 nm and these values have little influence on the simulation results. Therefore, here the monomer length is set to 1 nm. Fig.5-11 and Fig.5-12 show that both the elastic modulus and the viscosity influence the phase contrast and the indentation depth. When the viscosity is the same, the phase contrast and indentation depth decrease as the elastic modulus increases. This is because the larger modulus makes the tip stop and leave the surface faster with less damping. When the elastic modulus is G=1.0 MPa and G=10 MPa, the

phase contrast decreases as the viscosity increases. This is because the viscosity force is the dominant tip-surface interaction force and the increase of viscosity strongly influences the indentation depth of the tip and makes the tip stop and leave the surface faster. When the elastic modulus is G=0.1 GPa and G=1 GPa, the indentation depth decreases as viscosity increases from 0.1 Pa.s to 1 Pa.s but the phase contrast increases. This is probably because the tip stops faster but the smaller storage of energy gives the tip a smaller pull off speed. When viscosity is larger than 1 Pa.s, the phase contrast decreases again due to the tip staying less time on the PB surface. For elastic modulus E larger than 10 GPa, the elastic force is the dominant force and the viscosity has little influence on the phase contrast and the indentation depth.

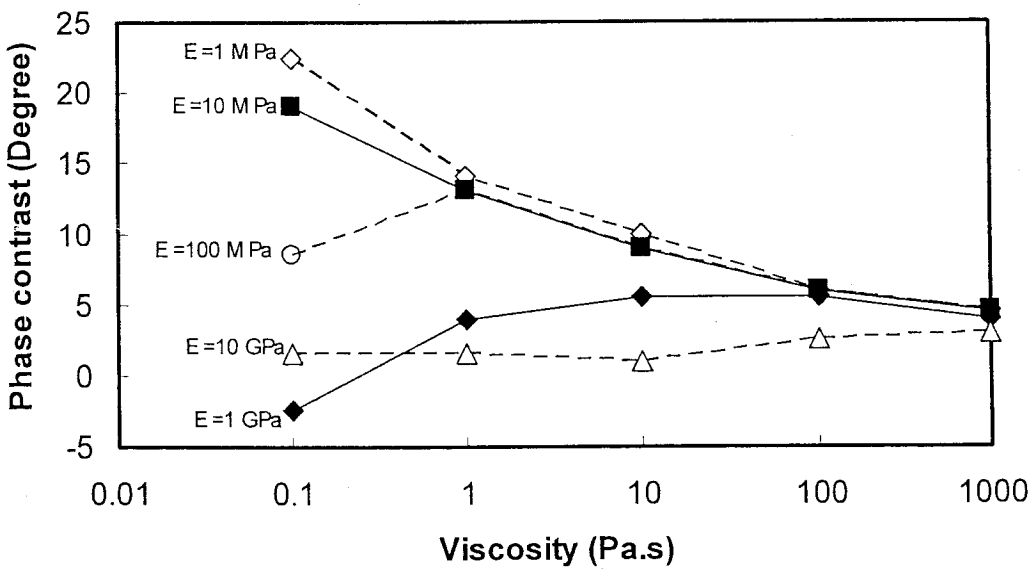

Figure 5-11 Simulated phase contrast with respect to silicon versus viscosity for different Young's modulus at a set point of 0.6, free amplitude 90 nm

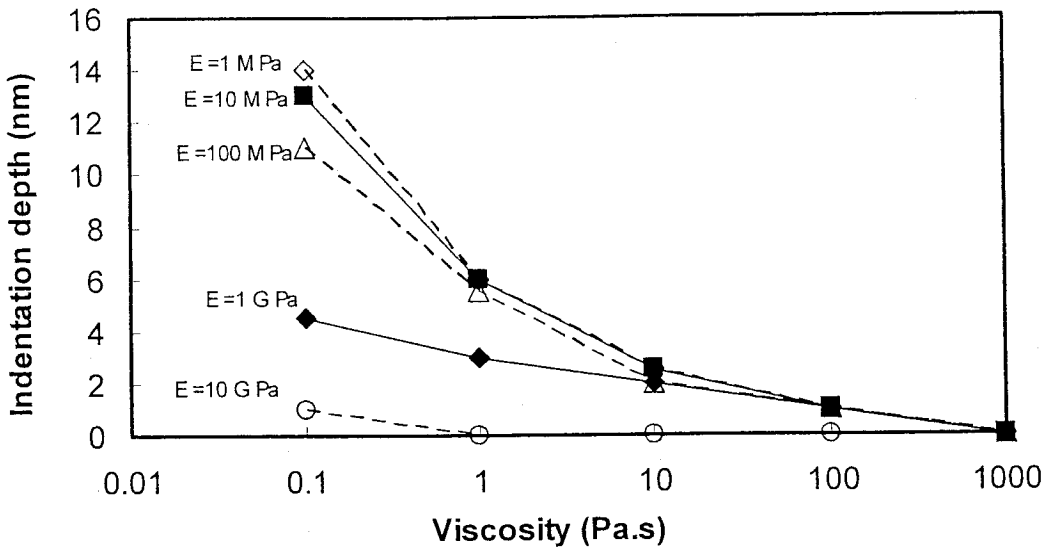

Figure 5-12 Simulated indentation depth versus viscosity for different Young's modulus at a set point of 0.6, free amplitude 90 nm

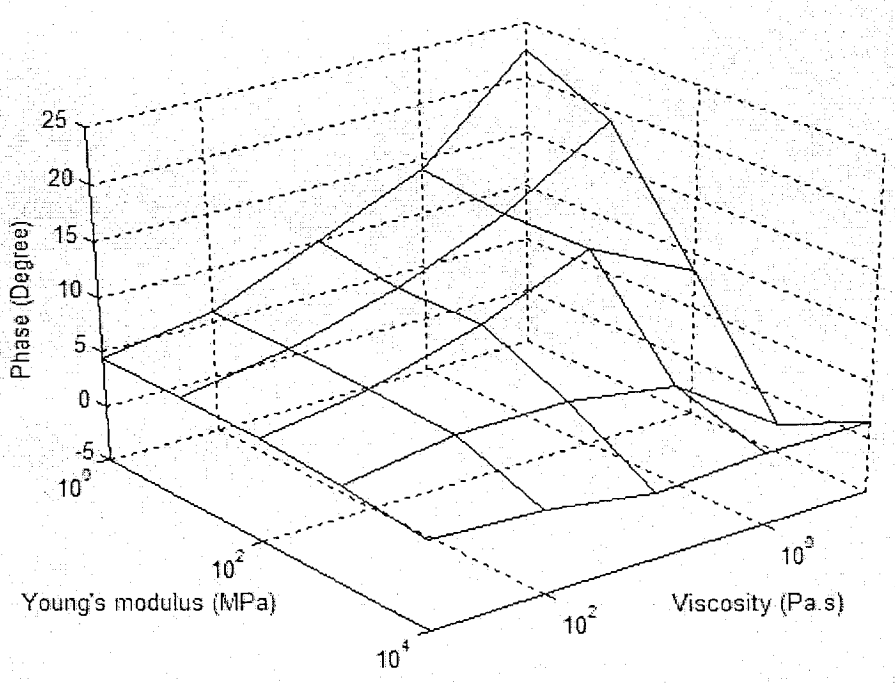

Figure 5-13 Phase contrast with respect to silicon as a function of Young's modulus and viscosity

Fig.5-13 shows that both the Young's modulus and the viscosity influence the phase image. According to Eq.1-7 and 1-8, the shear elastic modulus (G') and the viscosity are related by:

$$|\eta^*| = \sqrt{\left(\frac{G'}{\omega}\right)^2 + \left(\frac{G''}{\omega}\right)^2} \qquad [5.4]$$

At high ω frequencies such as those in AFM $G' >> G''$ and Eq.5-4 can be reduced to:

$$\eta = \frac{G'}{\omega} \qquad [5.5]$$

The time scale that the tip stays on the sample is about 10^{-7} s. Using Eq.5-5 we can estimate $\eta_m = G/10^7$. Therefore, Fig.5-11 can be reduced to Fig.5-14 which shows that the phase contrast is determined by the elastic modulus. The material properties can be determined directly from Fig.5-14 as we demonstrate later.

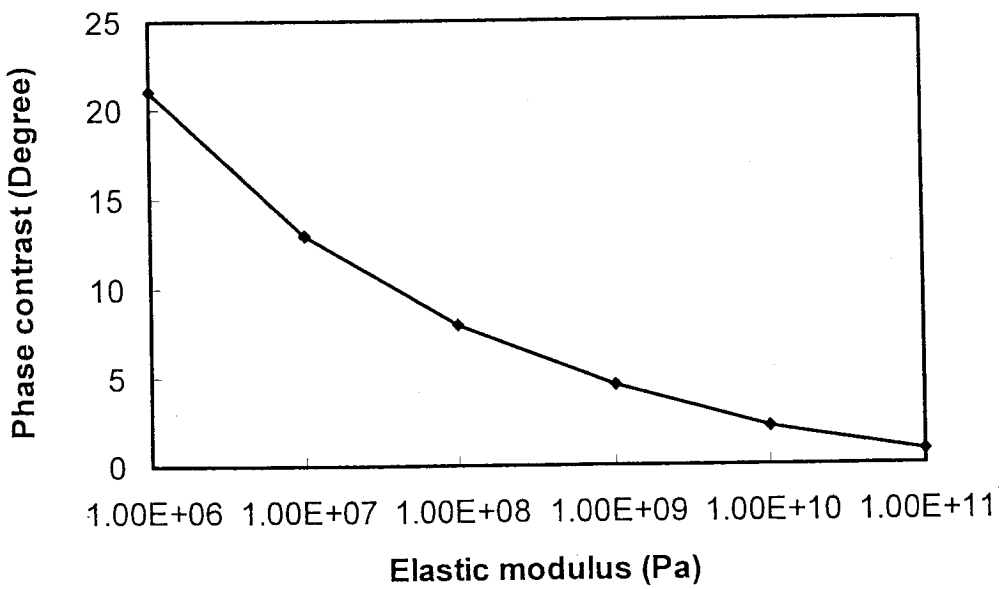

Figure 5-14 Simulated phase contrast versus Young's modulus for viscoelastic materials on silicon at a set point of 0.6, free amplitude 90 nm

6. Experimental results and discussion

6.1 Experimental results for PB on silicon

AFM images were obtained for PB films on a silicon surface when the Y direction scan was disabled. The PB film thickness was about 104 nm. By the method explained in the experimental methodology, we calculated the indentation depths and phase contrasts for different set points. The results are shown in Fig.6-1 and Fig.6-2. Simulation results are also shown for comparison.

When the set point is between 1.0 and 0.9, the phase contrast is negative. The reason for this is that the attracting force between the silicon atoms is larger than the force between atoms of silicon and PB. In some experiments, this negative phase contrast is not observed due to the unstable tip vibration under the influence of the attractive force. This is hard to predict by a model, because there are many factors such as the water layer, and the air flow between the surface and probe, which are difficult to control. When the set point is 0.9, the phase contrast has a small positive value meaning the average tip-sample interaction force is repulsive and small. The indentation depth can be seen as zero in this situation.

Fig.6-1 shows that the experimental indentation curve has the same shape as the simulation curve and is just shifted to the left slightly. This shift is caused by the van der Waals force between the tip and the sample surface which is under-estimated by the new model which does not consider the water layer. In Fig. 6-2 when the set point is between 0.5 and 0.8, the phase contrast agrees well with the simulation results. In this situation the tip-sample interaction is dominated by the repulsive forces that can be predicted by the new model. When the set point is 0.9-1.0, the dominant force is the attracting force and

our model fails because the water layer influence was not considered. When the set point is smaller than 0.5, the large interaction force makes the tip deflection complicated and the new model is not valid. These results demonstrate that if the set point is in the range of 0.5-0.8 the material properties can be predicted by combining the AFM phase image and our model.

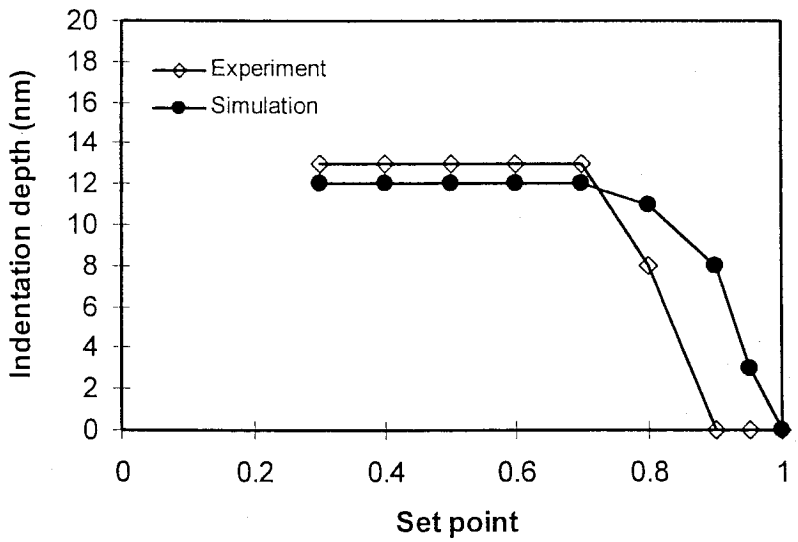

Figure 6-1 Indentation depth at different set points

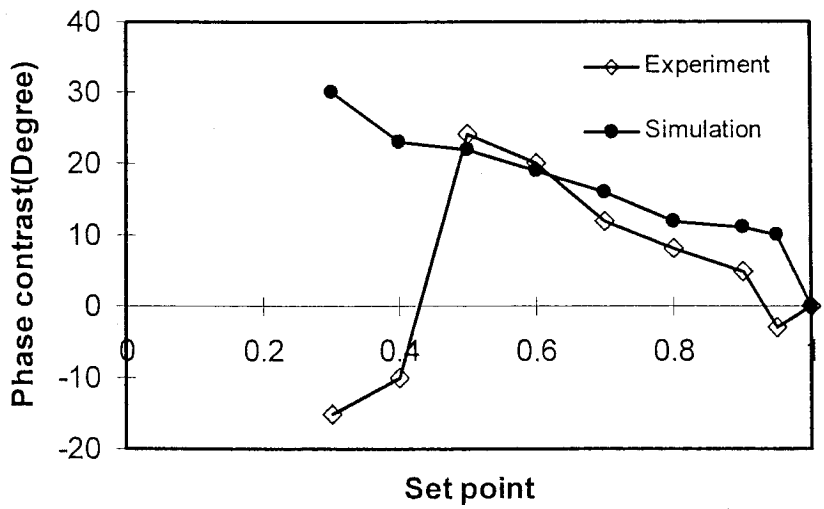

Figure 6-2 Phase contrast at different set points

6.2 The influence of polymer film thickness

To study the influence of polymer film thickness when the free amplitude is 90nm, we produced AFM images of a PB film with varying thickness. Fig. 6-3 shows the topography and phase image when the tip scans both the X and Y directions. The bright domain is the PB film and the dark domain is the silicon substrate.

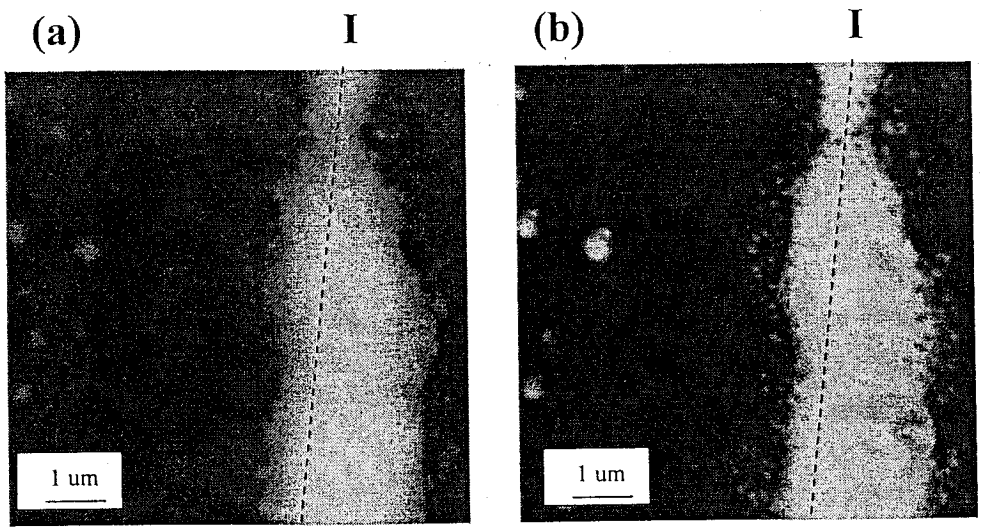

Figure 6-3 Topography image and phase image for PB on silicon surface at set point 0.6 free vibration amplitude 90nm. Grayscale is 0-300 nm for topography image and 0-50° for phase image

Fig.6-4 shows that the thickness changes from 20 nm to 162 nm along the line I of Fig.6-3a. Fig. 6-5 shows that the phase contrast decreases with increasing thickness when the PB film is thinner than 70 nm. But when the height of PB film is larger than 70 nm (point

a in Fig.6-4), the phase contrast of PB film is about 20 degrees and does not change with any further increases in thickness.

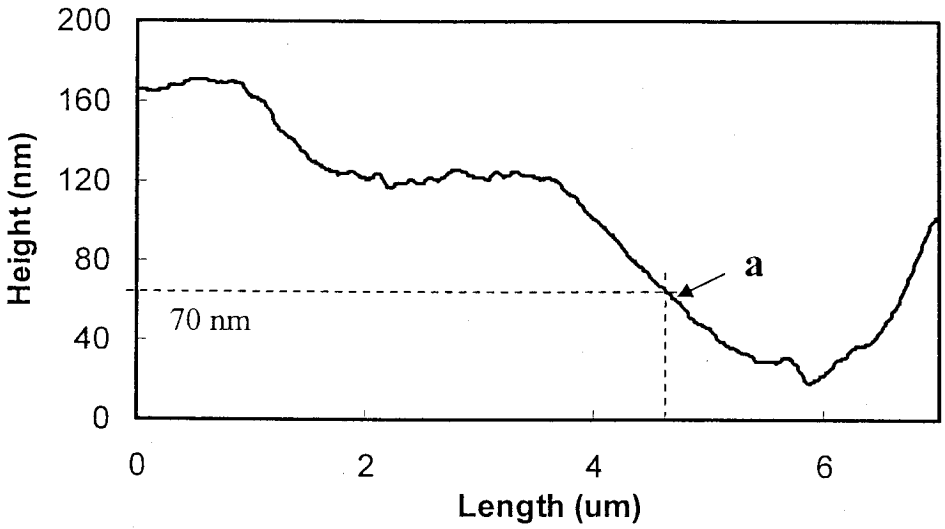

Figure 6-4 The topography section along line I of Fig.6-3a

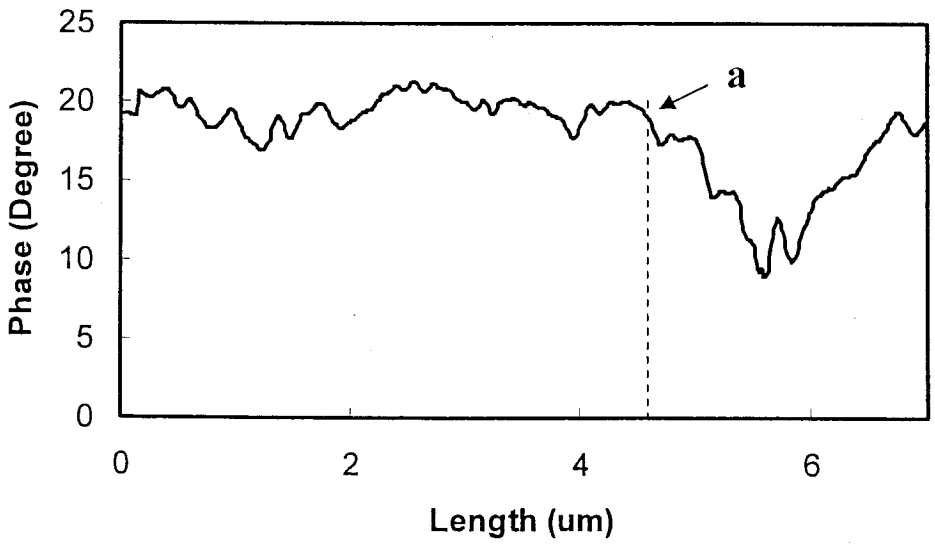

Figure 6-5 The phase section along line II of Fig.6-3b

70 nm is approximately the thickness for three molecules. Fig.6-6 shows how to estimate the thickness of one molecule.

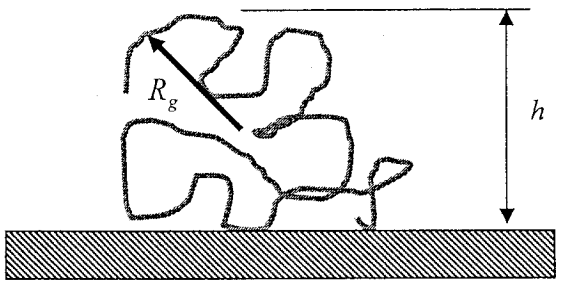

Figure 6-6 Calculation of the thickness of one molecule

$$h = 2R_g = 2\frac{b\sqrt{N}}{\sqrt{6}} \qquad [6\text{-}1]$$

where R_g is the radius of gyration, N the number of Kuhn monomers in one molecule and b the Kuhn monomer length. For the PB used here, $N = 714$, $b = 0.96$ nm, and the thickness of one molecule is $h \approx 21$ nm.

6.3 Experimental results for PS on silicon

AFM images were obtained for PS on the silicon surface. Fig.6-76 shows the results. The PS domain seems not to have the same shape in the topography image as in the phase image. This is because some of the PS film is too thin to be seen in the topography image, but in the phase image it can be seen.

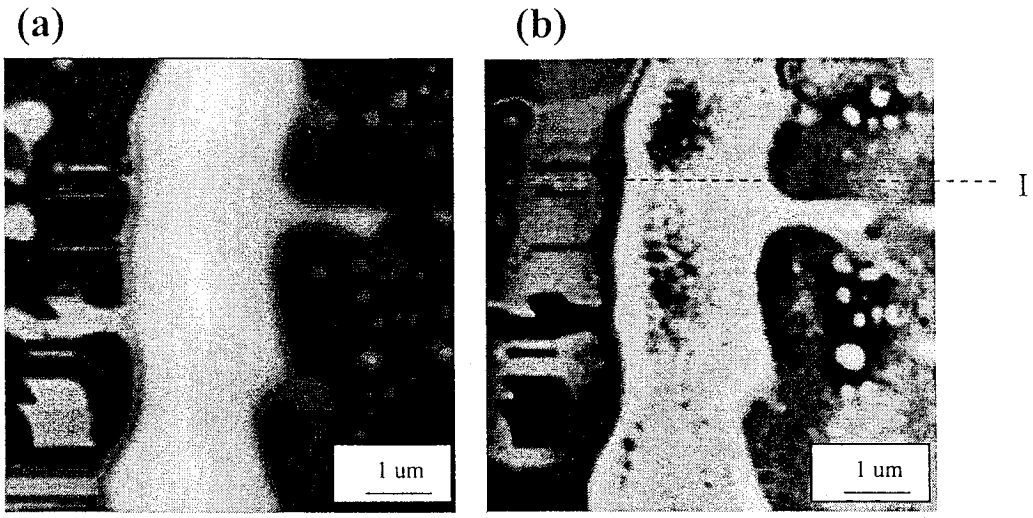

Figure 6-7 Topography and phase image of PS on silicon. Grayscale is 0-150 nm for topography image and 0-20° for phase image

Fig.6-8 shows the section along the line I in the image Fig. 6-7b. It shows that the phase contrast between PS and silicon is about 5 degrees. This agrees well with our simulation results.

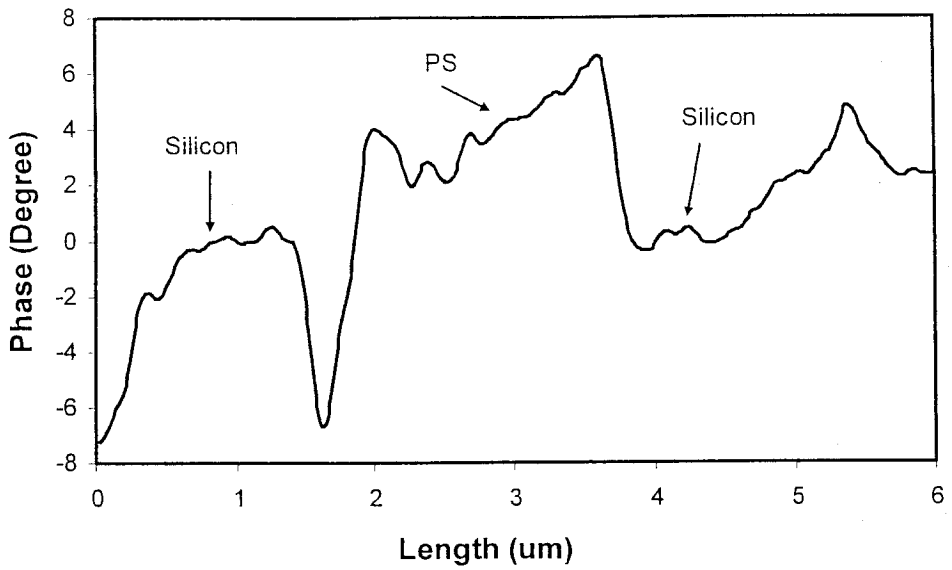

Figure 6-8 Phase image section along the line I in Fig.6-6

6.4 Experimental results for PB and PS on silicon

We also put PS and PB together on the silicon surface and produced the AFM images shown in Fig.6-9. The PB film thickness is about 500 nm and the PS thickness is about 700 nm.

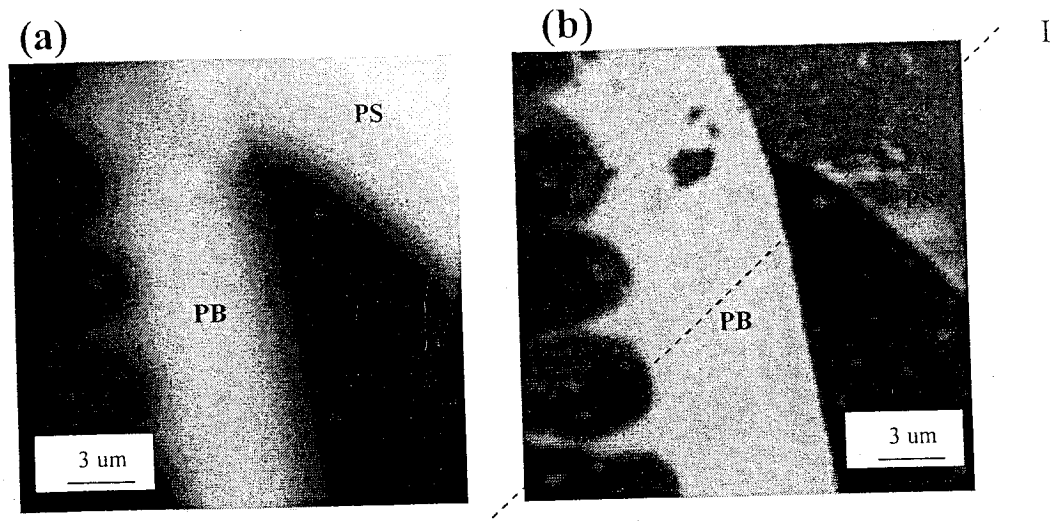

Figure 6-9 Topography (a) and phase (b) images of PS and PB on silicon at set point 0.6. Grayscale is 0-700 nm for topography image and 0-40° for phase image

Fig.6-10 shows that the phase contrast for PB and silicon is about 19 degrees and that for PS and silicon is about 5 degrees, this agrees well with the previous experimental results and with the simulation results.

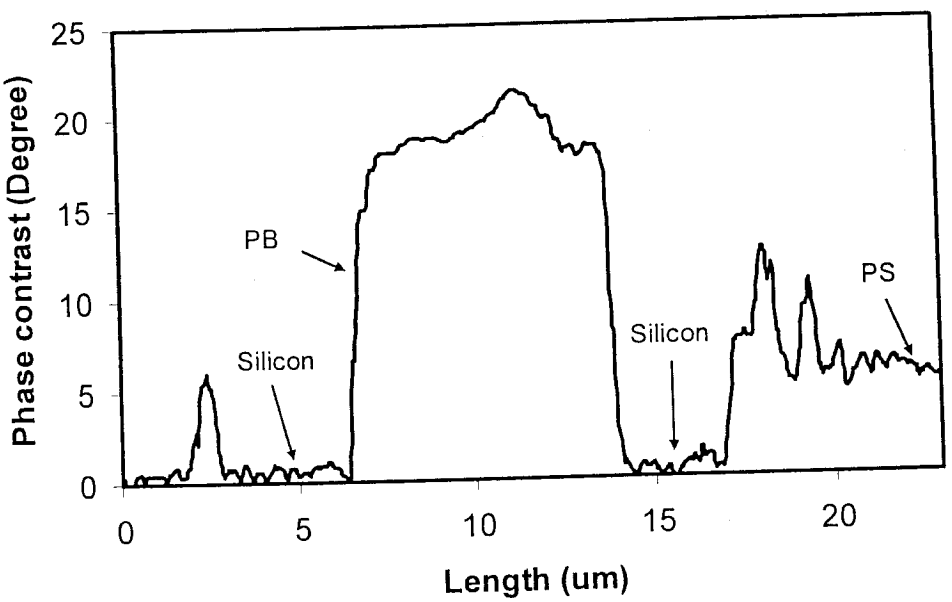

Figure 6-10 Topography section along the line I in Fig.6-9

7. Inferring material properties from the AFM phase image

7.1 PLLA

In order to evaluate the model, the analysis was applied to other materials. First poly-l-lactic acid (PLLA) was considered. Its solution was cast on a silicon surface and the AFM images were produced. Fig.7-1 shows that no crystals exist in the PLLA film. The topography image (a) clearly shows the PLLA film on the silicon surface, but in the phase image (b) the difference between the two regions is small.

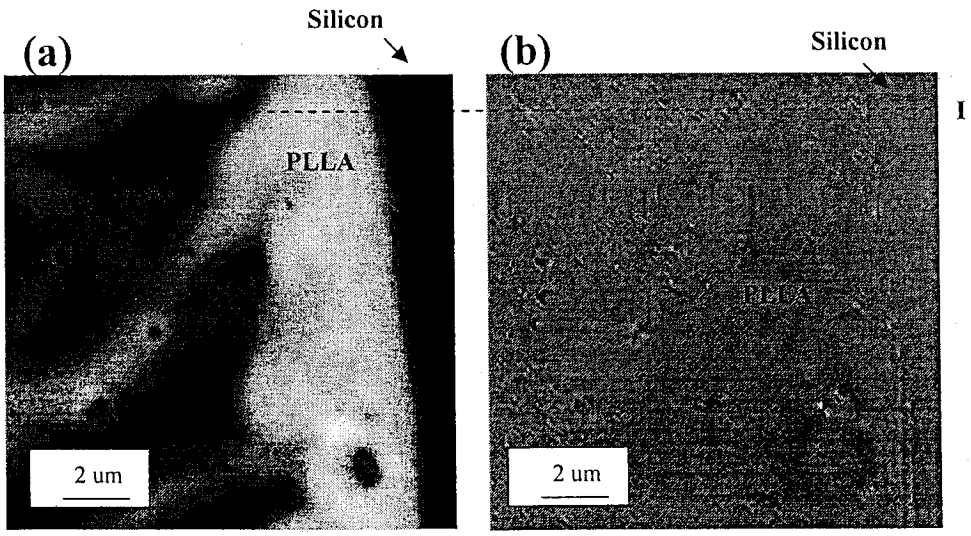

Figure 7-1 Topography and phase image for PLLA on silicon surface set point 0.6. Grayscale is 0-300 nm for topography image and 0-30° for phase image

Fig.7-2, which is a section along line I in Fig.7-1, shows that the phase contrast between PLLA and silicon is about 1.5 degrees. This means the PLLA is harder than PB and PS. In Fig. 7-2, we also see the topography causes some interference on the phase image when the topography changes slope. This is because the scanner will continue to move a certain distance according to the original slope before the feed back loop adjusts it. A good controller gain value can minimize this influence.

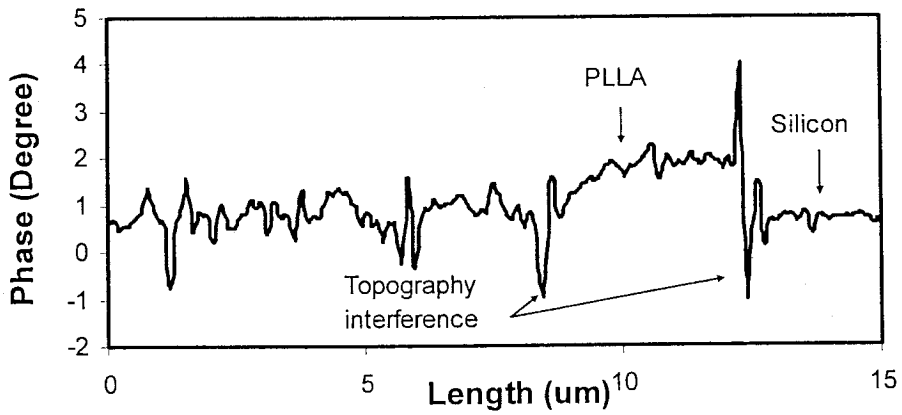

Figure 7-2 Phase section along the line I in Fig.7-1

In order to observe crystals we annealed the PLLA film at 140℃ for 2 minutes and then produced the AFM images again. In Fig.7-3, both the phase and topography images show that crystals appear on the PLLA surface after annealing. The topography and the phase of the crystal region and the amorphous region are different. Fig.7-4 shows that the phase contrast for the crystal region is about 1.2 degree higher than that of the amorphous region. This means the crystal of the PLLA is a little softer than the amorphous region

which is glassy, but both of them are harder than PS and PB. Fig. 7-5 shows that topography did not influence the phase image significantly.

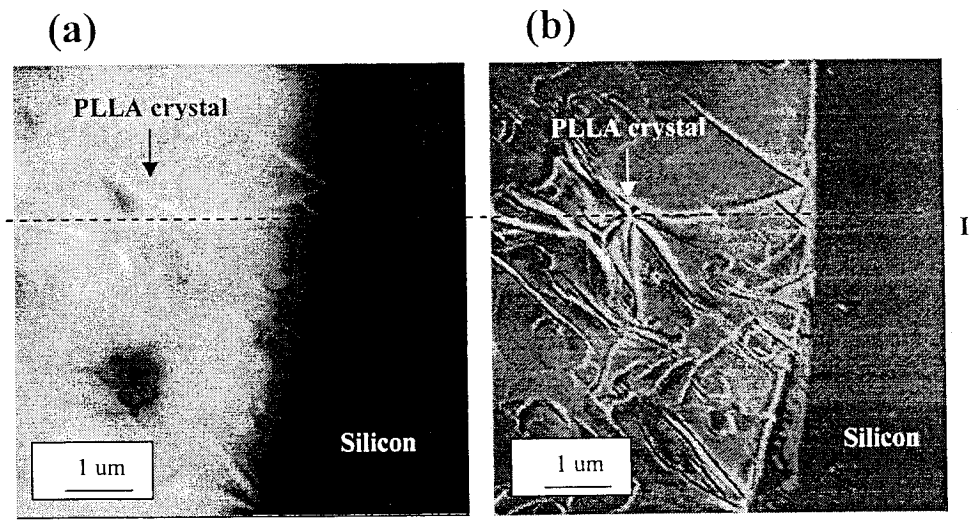

Figure 7-3 Topography and phase image for PLLA on silicon surface after annealing set point 0.6. Grayscale is 0-300 nm for topography image and 0-10° for phase image

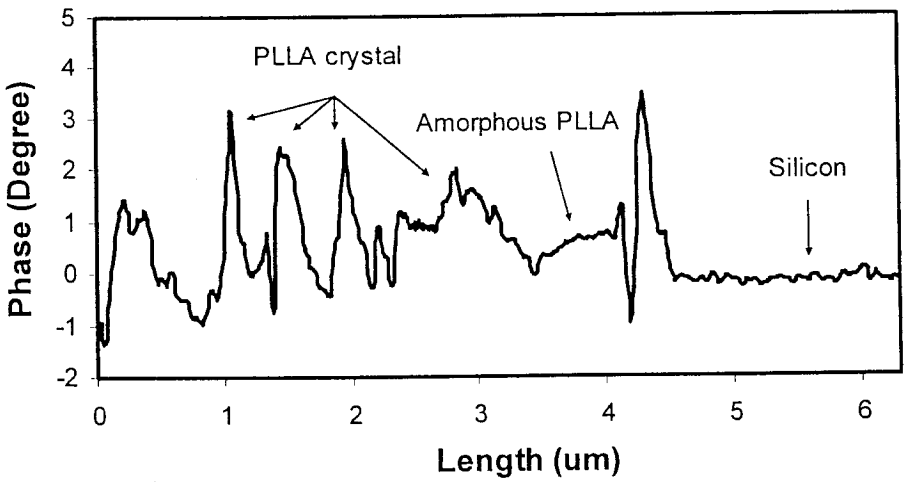

Figure 7-4 Phase section along the line I in Fig.7-3

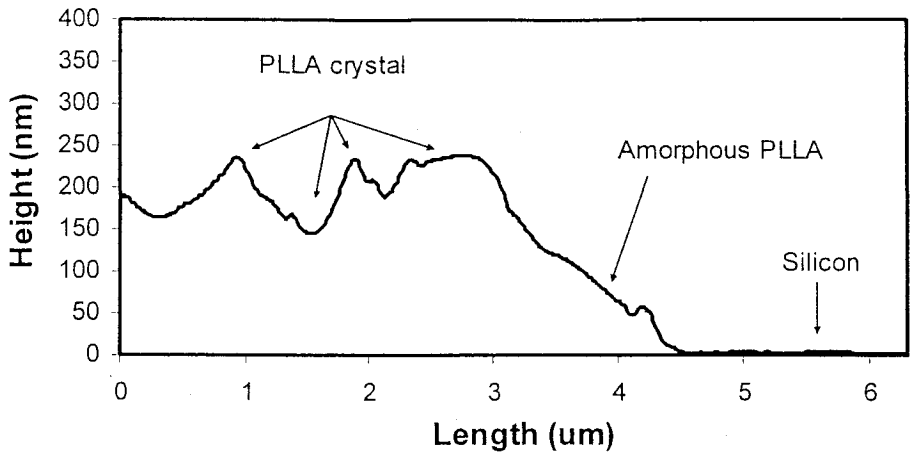

Figure 7-5 Topography section along the line I in Fig.7-3

7.2 PB-PS-PB Block copolymer

To study the block copolymer properties we cast a Polybutadiene-Polystyrene-Polybutadiene (PB-PS-PB) block copolymer on the silicon surface and produced AFM images. Fig.7-6 clearly shows the block copolymer on the silicon surface. Fig.7-7 shows that the phase contrast between the block copolymer and silicon is about 15 degrees which is between those of pure PB and PS. This means the block copolymer is a little harder than PB and softer than PS.

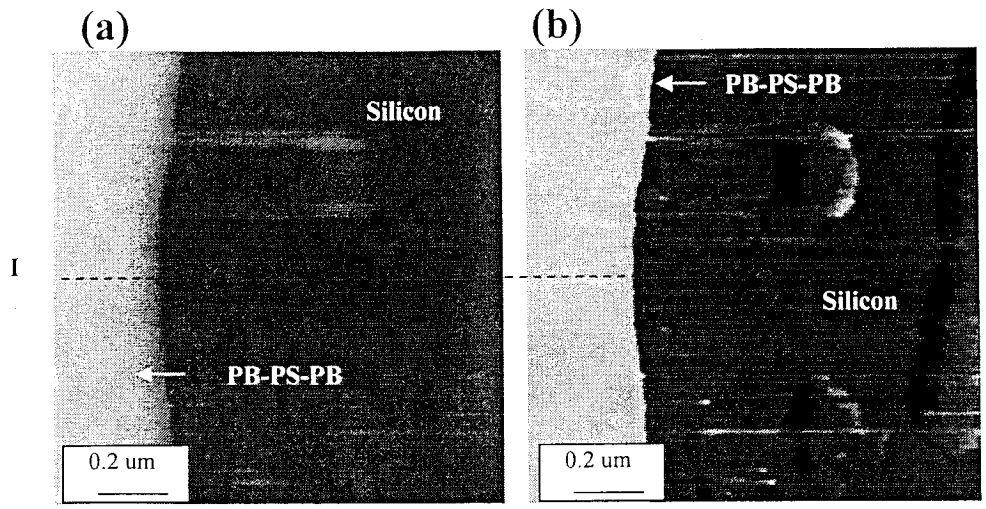

Figure 7-6 Topography and phase image for PB-PS-PB copolymer on silicon surface without annealing set point 0.6. Grayscale is 0-300 nm for topography image and 0-40° for phase image

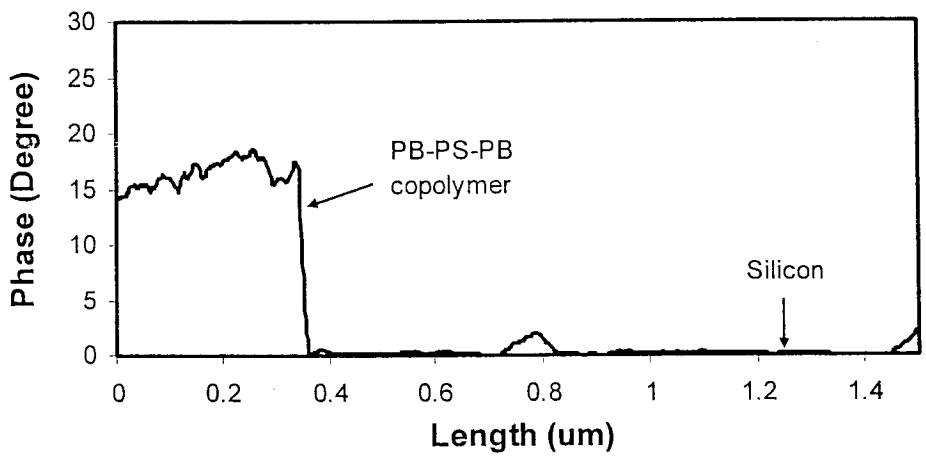

Figure 7-7 Phase section along the line I in Fig.7-6

Next we annealed the PB-PS-PB block copolymer at 140℃ for 30 minutes to allow for micro-phase separation and then produced the AFM images. Fig. 7-8 shows that the color of the copolymer film region becomes uneven. This means that domains with different material properties appear within the polymer film. Fig.7-9 shows that the phase difference for the different domains is very large. The largest phase contrast relative to silicon is 22° and the smallest is 3°. This is because the annealing allowed the PS and PB blocks come to together and form PS and PB domains. Each domain has the same mechanical properties as its single chain polymer.

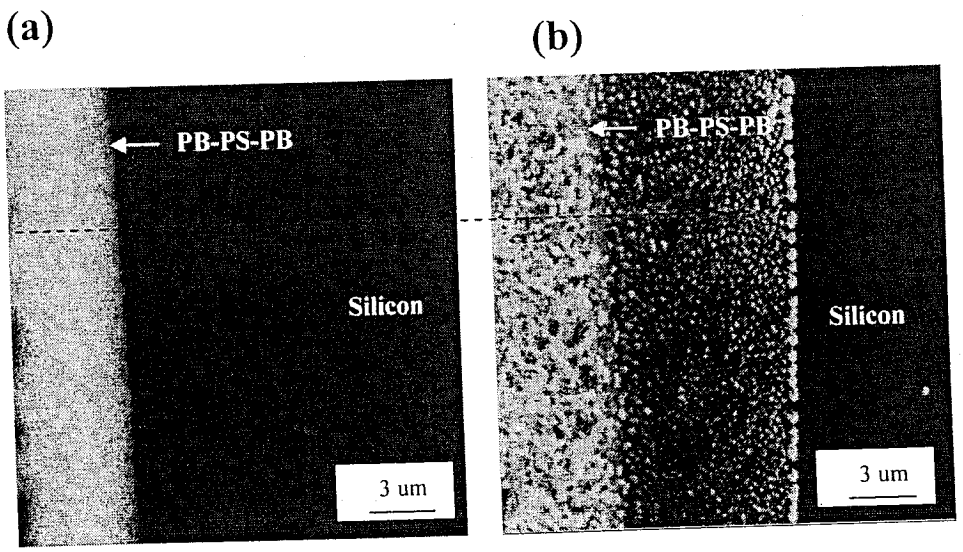

Figure 7-8 Topography and phase image for PB-PS-PB copolymer on silicon surface after annealing. Grayscale is 0-300 nm for topography image and 0-40° for phase image

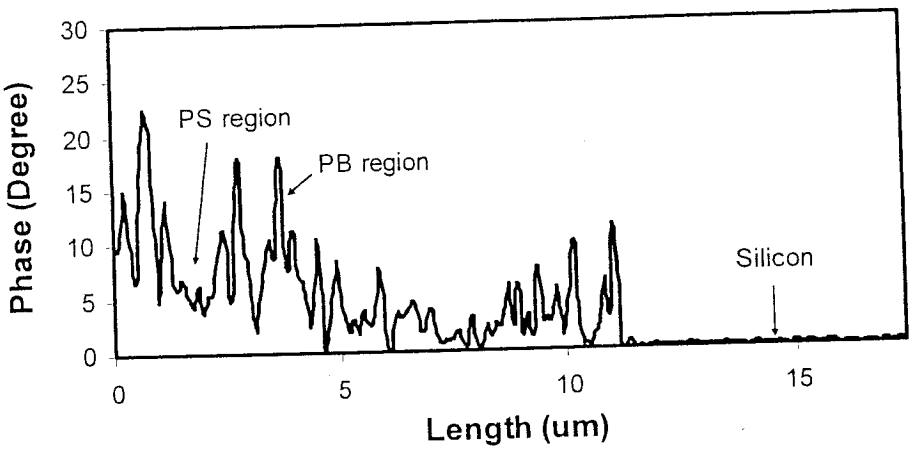

Figure 7-9 Phase section along the line I in Fig.7-8

7.3 Comments

Fig. 7-10 shows the material properties that were inferred from the phase contrast between the various materials and silicon using Fig. 5-14. The elastic modulus of PB and PS inferred from the phase contrast is 1.3 MPa and 0.9 GPa, these agree well with the bulk properties. But for the PLLA, the modulus inferred is 30 GPa, which does not agree well with the material specification. The reason for this is that when the phase contrast is smaller than 5 degrees, the error becomes large; and the values of phase contrast of PLLA and silicon range is from 1 to 4 degrees.

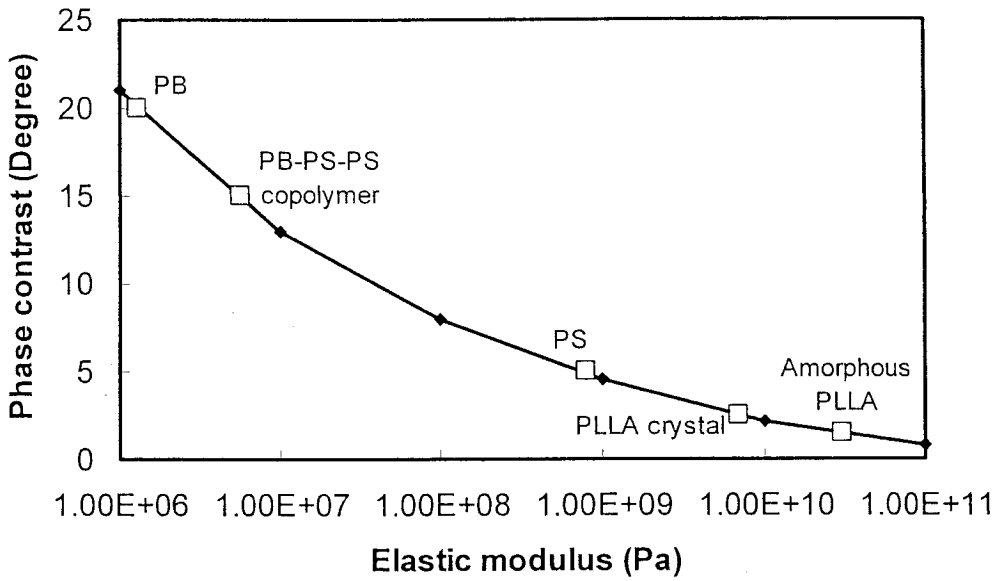

Figure 7-10 Inferring material properties

8. Detecting material properties beneath the Polymer films

In section 6.1, it was proved that when the free vibration amplitude is 90 nm, the set point is 0.6, and the thickness of the PB film is larger than 70 nm, the thickness of PB film has no influence on the phase image. When the free vibration amplitude increases, this critical thickness increases. This is because the increased interaction force makes the tip influence the material deeper under the surface. Therefore if the material's property is different beneath the surface, the AFM can detect this difference. To study this, a PB solution was cast on the silicon grid and the AFM images were produced. Fig. 8-1 shows the geometry of the PB film on the silicon grid.

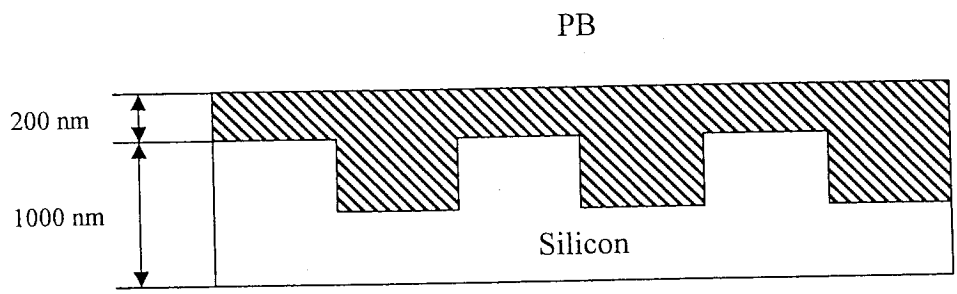

Figure 8-1 The PB film on silicon surface where the AFM images in Fig.82 were taken

Fig. 8-2 shows the topography image and phase image when the tip-sample interaction force is very large. Image (a) shows no topography change. But in the phase image (b), the phase difference shows the shape of the silicon grid. This is because the step of the silicon grid makes the PB film thickness uneven. The thinner region is stiffer

than the thicker region. Fig. 8-3 shows that the phase of the thinner region is about 0.5 degree smaller than that of the thicker region.

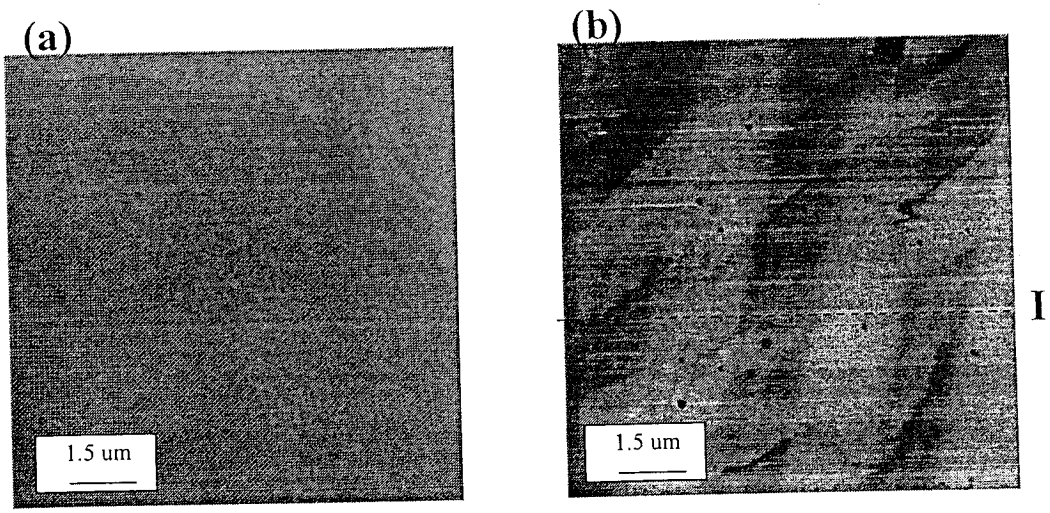

Figure 8-2 Topography and phase image of PS on silicon free amplitude 180 nm, set point 0.6. Grayscale is 0-100nm for topography image and 0-5° for phase image

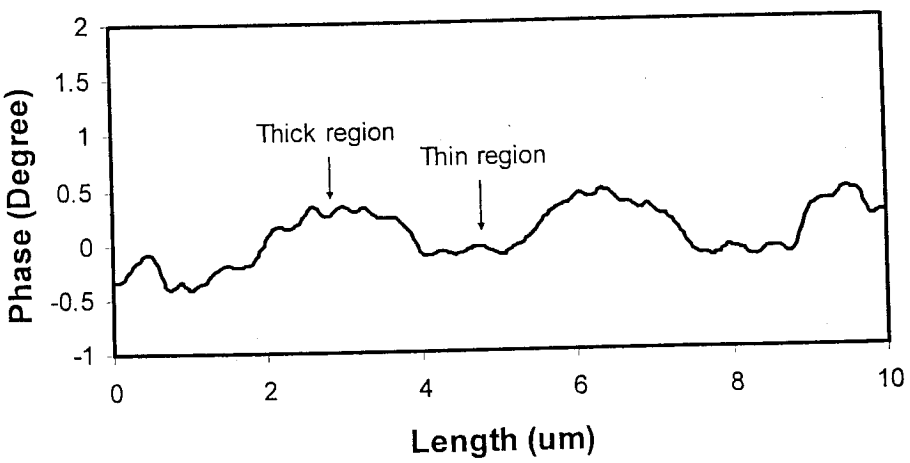

Figure 8-3 Phase section along the line I in Fig. 8-2

9. Conclusions

The influences of local material properties on tapping mode AFM are studied in this thesis. The simulation and experimental results show that this influence can be described for viscoelastic materials by a mathematical model given the material's mechanical properties. This gives us a way to infer properties of an unknown material with nanometer resolution, which can not be obtained by other means. We can also obtain information about the material structure on the nanometer scale using our approach. By comparing the AFM phase image of a material before and after external processing, we can find the change of material structure and properties on the nanometer scale.

10. Contributions

A new model was developed to describe the influences of material properties on the phase image of TM-AFM. A new method to obtain the material properties from the phase contrast between materials and silicon on the tapping mode AFM phase images was developed. It is also demonstrated experimentally that tapping mode AFM can detect the material properties beneath polymer films.

11. Future work

11.1 Simulations

In the model developed in this thesis the viscosity changes with the ratio of the indentation depth and the monomer length. It is more reasonable to use an instantaneous viscosity that changes with time during the tip-sample contact because this is a more realistic representation of viscoelastic flow. Moreover, it is possible that the elastic modulus also changes within the tip-sample contact time scale therefore this need to be incorporated into the model.

More simulations can also be done using different probe spring constants and quality factors. Then the simulation results for different tips can be obtained and used to decide the best parameters of probe that diminish the influences of other factors.

11.2 Experiment

Bulk rheology experiments need to do with the PS to obtain more accurate material properties. Also both AFM experiments and rheholgy experiments could be performed for other materials to evaluate the model developed in this work. Tips with different spring constants and quality factors can be used in the AFM experiments. By comparing the simulation results and the experiment results, the best tip parameters can be determined. To decrease the influence of the water layer, experiments can be done in water and the corresponding parameters can be incorporated into the simulation. To develop a new technology to obtain the material properties from the AFM phase image, it is necessary to define a standard for the parameters of the probe. These parameters include the probe material, dimensions, tip radius, and spring constant. The best

parameters can be determined from simulations and experiments. The standard tip should be well represented by the simulations and should diminish the influence of other factors in experiments.

Reference

1. Ricardo Garcia, Ruben perez, *Dynamic atomic force microscopy methods,* Surface Science Report, **2002**, vol.47, 197–301.
2. Sergei S. Sheiko, *Imaging of polymers using scanning force microscopy: From superstructures to individual molecules*, Advances in Polymer Science, Springer-Verlag Berlin Heidelberg, **2000**, vol.151, 62-159.
3. Georg Bar, Rainer Brandsch, Myung-Hwan Whangbo, *Effect of Viscoelastic properties of polymers on the phase shift in tapping mode atomic force microscopy*, Langmuir, **1998**, vol.14, 7343-7347.
4. Alexandre Berquanda, Pierre-Emmanuel Mazerana, Jean-Marc Laval, *Influence of volume and surface properties on phase contrast,* Surface Science, **2003**, vol.523, 125–130.
5. D. Raghavan, M. Vanlandingham, X. Gu, T., *Nguyencharacterization of Heterogeneous Regions in Polymer systems using tapping mode and force mode atomic force microscopy*, Langmuir, **2000**, vol.16, 9448-9459.
6. Lugen Wanga, *Analytical descriptions of the tapping-mode atomic force microscopy response,* Applied Physics Letters, **1998**, vol.73, Number 25.
7. Farida Benmouna and Diethelm Johannsmann, *Viscoelasticity of Gelatin Surfaces Probed by AFM Noise Analysis,* Langmuir, **2004**, vol.20, 188-193.
8. M. Sakai, *Time-dependent viscoelastic relation between load and penetration for an axisymmetric indenter*, Philosophical Magazine A, **2002**, vol.82, No.10, 1841-1849.

9. Bernhard Basnar, Germot Friedbacher, Helmut Brunner, Thomas Vallant, Ulrich Mayer, Helmuth Hoffmann, *Analytical evaluation of tapping mode atomic force microscopy for chemical imaging of surfaces*, Elsevier, **2001**, vol.171, 213–225.

10. P. J. James, M. Antognozzi, J. Tamayo, T. J. McMaster, J. M. Newton, and M. J. Miles, *Interpretation of Contrast in Tapping Mode AFM and Shear Force Microscopy. A Study of Nafion,* Langmuir, **2001,** vol.17, 349-360.

11. Alvaro San Paulo and Ricardo Garcı´a, *Tip-surface forces, amplitude, and energy dissipation in amplitude-modulation force microscopy,* Physical Review B, **2001,** vol. 64, 193411-1-4.

12. M. Marth, D. Maier, and J. Honerkamp, *A unifying view on some experimental effects in tapping-mode atomic force microscopy*, Journal of Applied Physics, **1999**, vol.85, Number 10, 7030-7036.

13. You Wang, Rui Song, Yingshum Li, Jingshu Shen, *Understanding tapping-mode atomic force microscopy data on the surface of soft block copolymers*, Elsevier, **2003**, vol.530, 136–148.

14. L. Delineau, R. Brandsch, G. Bar, M.-H. Whangbo, *Harmonic responses of a cantilever interacting with elastomers in tapping mode atomic force microscopy*, Surface Science, **2000**, vol.448, 179-187.

15. William W. Scott, Bharat Bhushan, *Use of phase imaging in atomic force microscopy for measurement of viscoelastic contrast in polymer nanocomposites and molecularly thick lubricant films*, Elsevier Science, **2003**, vol.97, 151-169.

16. Faith. A. Morrison, *Understanding Rheology,* Oxford University Press, **2001**

17. Michael Rubinstein, Ralph h. Colby, *Polymer Physics,* Oxford University Press, Oxford, **2003**.

18. William T. Thomson, Marie Dillon Dahleh, *Theory of Vibration with Applications*, Prentice Hall, **1998.**

19. Jeffery P. Hunt and Dror Sarida, *Kinetics of lossy grazing impact oscillators*, Applied Physics Letters, **1998**, vol.72, Number 23, 2969-2971

20. J. Tamayo, R. Garcia, *Deformation, contrast, and phase contrast in tapping mode scanning force microscopy*, Langmuir, **1996**, vol.12, 4430-4435.

21. Ricardo Garcia, Alvaro San Paulo, *Attractive and repulsive tip-sample interaction regimes in tapping-mode atomic force microscopy*, Physical Review B, **1991**, vol.60, Number 7, 4961–4967.

22. Robert W. Stark, Georg Schitter, and Andreas Stemmer, *Tuning the interaction forces in tapping mode atomic force microscopy*, Physical Review, **2003**, vol.68, 085401.

23. F. Dubourg, J.P. Aime, S. Marsaudon, R. Boisgard, and P. Leclere, *Probing viscosity of a polymer melt at the nanometer scale with an oscillating nanotip*, The European Physical Journal, **2001**, vol.E6, 49-55.

24. F. Dubourg, S. kopp-Marsaudon, Ph. Leclere, R. Lazzaroni, and J.P. Aime, *Experimental determination of the viscosity at the nanometer scale on a block copolymer with an oscillating nanotip*, The European Physical Journal, **2001**, vol.E6, 387-397.

25. J.P. Cleveland, B. Anczykowski, A.e. Schmid, V.B. Elings. Appl. Phys. **1998**, vol.72, Number 20, 2613.

26. C.G. Robertson, *Bridgestone/Firestone Research Private report,* **2004**

Appendix
Simulation system